CAIT-UTC-REG49

Post-fire Damage Assessment of Concrete Tunnel Liners

FINAL REPORT
August 2022

Submitted by:

Negar Elhami-Khorasani
Associate Professor

Anthony Tessari
Associate Professor

Department of Civil, Structural and Environmental Engineering
University at Buffalo

External Project Manager:

Harry Capers, Vice President
Arora and Associates, P.C.

In cooperation with

Rutgers, The State University of New Jersey
And
U.S. Department of Transportation
Federal Highway Administration

Disclaimer Statement

The contents of this report reflect the views of the authors, who are responsible for the facts and the accuracy of the information presented herein. This document is disseminated under the sponsorship of the Department of Transportation, University Transportation Centers Program, in the interest of information exchange. The U.S. Government assumes no liability for the contents or use thereof.

The Center for Advanced Infrastructure and Transportation (CAIT) is a Regional UTC Consortium led by Rutgers, The State University. Members of the consortium are Atlantic Cape Community College, Columbia University, Cornell University, New Jersey Institute of Technology, Polytechnic University of Puerto Rico, Princeton University, Rowan University, SUNY - Farmingdale State College, and SUNY - University at Buffalo. The Center is funded by the U.S. Department of Transportation.

1. Report No.	2. Government Accession No.	3. Recipient's Catalog No.
CAIT-UTC-REG49		

4. Title and Subtitle	5. Report Date
Post-fire Damage Assessment of Concrete Tunnel Liners	July 2022
	6. Performing Organization Code CAIT/University at Buffalo

7. Author(s)	8. Performing Organization Report No.
1. Nan Hua https://orcid.org/0000-0002-3046-9331 2. Marzieh Shahraki https://orcid.org/0000-0001-8142-5374 3. Anthony Tessari https://orcid.org/0000-0003-0231-345X 4. Negar Elhami-Khorasani https://orcid.org/0000-0003-3228-0097	CAIT-UTC-REG49

9. Performing Organization Name and Address	10. Work Unit No.
University at Buffalo, Department of Civil, Structure and Environmental Engineering 212 Ketter Hall, Buffalo, NY, 14260	11. Contract or Grant No. 69A3551847102

12. Sponsoring Agency Name and Address	13. Type of Report and Period Covered
Center for Advanced Infrastructure and Transportation Rutgers, The State University of New Jersey 100 Brett Road, Piscataway, NJ 08854	Final Report 02/01/2021 – 07/31/2022
	14. Sponsoring Agency Code

15. Supplementary Notes
U.S. Department of Transportation/OST-R
1200 New Jersey Avenue, SE, Washington, DC 20590-0001

16. Abstract

Extreme fire events in tunnels may have catastrophic consequences, which include loss of life, structural damage, and major socioeconomic impacts due to service disruptions. This report focuses on post-fire damage assessment of reinforced concrete tunnel liners and provides recommendations on damage assessment procedures for application in practice. A review of experimental post-fire residual mechanical properties, primarily organized and sorted based on aggregate type and soak time, are presented. The normalized residual concrete strength results are compared to Eurocode. The reduction factors for siliceous aggregate are approximately equivalent to the median of the data, whereas the Eurocode reduction factors are likely unconservative for calcareous aggregate, although more data is needed to confirm. Two continuous temperature-dependent probabilistic models, for residual concrete strength with siliceous and calcareous aggregates are developed for use in numerical simulations. Further, this report describes a series of finite element analyses on realistic tunnel sections within soil or rock profiles. Four tunnel-soil combinations are presented: shallow and soft soil, moderate depth and soft soil, moderate depth and rock, and deep depth and rock. Post-fire residual deformations and stresses within concrete liner are studied. The model for soft soil captures temperature-dependent excess pore water generation and thermal hardening. Upper and lower bounds of modulus of elasticity for models containing temperature-dependent soils are presented, although more data is needed for other soil or rock types. Finally, this report details a framework for the damage assessment of concrete tunnels following a fire, considering ad-hoc processes, advanced modelling, data collected from stakeholders, and published classification and damage thresholds. The framework quantifies fire damage to tunnel linings in terms of surface discoloration, crack width, concrete spalling, sectional temperatures, strength loss of materials, and residual displacement. A case study is presented, and a damage classification system is proposed to systematically map damage metrics to repair strategies.

17. Key Words	18. Distribution Statement
Tunnel, concrete liner, fire, damage	

19. Security Classification (of this report)	20. Security Classification (of this page)	21. No. of Pages	22. Price
Unclassified	Unclassified	77	

Form DOT F 1700.7 (8-69)

Acknowledgments

The authors gratefully acknowledge the Region 2 UTC Consortium led by the Center for Advanced Infrastructure and Transportation (CAIT) at the Rutgers University and the Institute of Bridge Engineering (IBE) at the University at Buffalo for their generous support. Any opinions, findings, and conclusions, or recommendations expressed in this material are those of the authors and do not necessarily reflect the views of the CAIT Region 2 UTC Consortium.

The authors would like to thank Professor Maria Garlock of Princeton University, who served as the project collaborator and provided advice on the technical research approach. The inputs and guidance of Mr. Harry Capers, the primary project stakeholder, are greatly appreciated.

Table of Contents

CHAPTER 1 INTRODUCTION 9

1.1 Motivation 9

1.2 Objective and scope 10

CHAPTER 2 POST-FIRE RESIDUAL STRENGTH OF CONCRETE 12

2.1 Methodology 12

2.1.1 Material collection 13

2.1.2 Description analysis 13

2.1.3 Category selection 14

2.2 Material evaluation 15

2.2.1 Effect of course aggregate 15

2.2.2 Effect of testing protocol 18

2.3 Probabilistic model for post-fire residual strength of concrete 23

2.3.1 Evaluate candidate distributions 23

2.3.2 Temperature-dependent parameters of the Weibull distribution 27

2.4 Conclusion 30

CHAPTER 3 INFLUENCE OF SOIL CONDITIONS ON DAMAGE TO TUNNEL STRUCTURES AFTER FIRE 32

3.1 Representative geologic profiles for realistic tunnel sections 33

3.1.2 Tunnel section 1: a shallow section in soft soil 33

3.1.3 Tunnel section 2: a moderate-depth section in soft soil 34

3.1.4 Tunnel section 3: a moderate-depth section in rock 35

3.1.5 Tunnel section 4: a deep section in rock 35

3.2 Model verification and reinforcement design for tunnel sections 36

3.2.1 Verification of the beam-spring model 36

3.2.2 Reinforcement design 39

3.3 Fire performance of the tunnel sections: methodology 40

3.3.1 RABT-train fire curve 41

3.3.2 RWS fire curve 43
3.3.3 Effect of temperature on soil properties 43
3.4 Results 46
3.4.1 RABT-train fire curve 46
3.4.2 RWS fire curve 50
3.4.3 Effect of temperature on soil properties 51
3.5 Conclusion 52
CHAPTER 4 DAMAGE ASSESSMENT 54
4.1 Introduction 54
4.2 Framework 54
4.2.2 Guided post-fire damage assessment procedure 55
4.2.3 Advanced modelling 57
4.2.4 Damage classification and repair requirement 58
4.3 Case study 61
4.3.1 Test parameters 61
4.3.2 Numerical modelling 63
4.3.3 Damage assessment 65
4.4 Conclusion 66
CHAPTER 5 CONCLUSIONS AND RECOMMENDATIONS 67

List of Figures

Figure 1.1 General procedure for fire damage assessment 10
Figure 2.1 Distribution of specimen type in the collected data 14
Figure 2.2 Collected parameters that could influence residual compressive strength of concrete exposed to high temperatures 14
Figure 2.3 Normalized residual strength of concrete as a function of temperature for experimental data and the Eurocode 2 reduction factors for (a) siliceous and (b) calcareous aggregate types 17
Figure 2.4 Normalized residual strength of concrete with (a) siliceous and (b) calcareous aggregates categorized based on different heating rate (*or ASTM E119) 19
Figure 2.5 Normalized residual compressive strength of concrete with siliceous aggregate and retaining time (a) less than or equal to 2 hours, (b) greater than to 2 hours 21
Figure 2.6 Normalized residual strength of concrete with calcareous aggregate and retaining time (a) less than or equal to 2 hours, (b) greater than to 2 hours 22
Figure 2.7 Grouped data points for concrete with (a) siliceous (b) calcareous aggregates 24
Figure 2.8 Comparison of the mean criterion value for each of the 13 candidate PDF models for the residual compressive strength of concrete with (a) siliceous (401 points) and (b) calcareous (159 points) aggregates 26
Figure 2.9 Selected probabilistic models along with PDF for normalized residual strength for (a) siliceous and (b) calcareous concrete data at 200°C, 300°C, and 400°C 27
Figure 2.10 Temperature-dependent polynomial regression for λ and k representing (a) siliceous concrete and (b) calcareous concrete 29
Figure 2.11 Temperature-dependent residual strength data for normal strength concrete versus the Weibull probabilistic model and EC2 reduction factors for: (a) siliceous concrete, and (b) calcareous concrete 30
Figure 3.1 Geologic profile for tunnel section 1 (data from (Ngan et al., 2017)) 34
Figure 3.2 Geologic profile for tunnel section 2 (data from (BTS, 2004)) 34
Figure 3.3 Geologic profile for tunnel section 3 (data from (BTS, 2004)) 35
Figure 3.4 Geologic profile for tunnel section 4 (data from (BTS, 2004)) 36
Figure 3.5 (a) FLAC3D model and (b) SAFIR model for the sample tunnel section 37
Figure 3.6 Comparison of results between Elastic Equation Method, SAFIR, and FLAC3D based on (a) bending moment and (b) axial force in the tunnel section 39
Figure 3.7 The RABT-train and RWS fire temperature-time curves 41
Figure 3.8 The beam-spring model for the mechanical analysis under fire 42
Figure 3.9 Considered changes in soil behavior under elevated temperatures for application in the structural analysis of tunnel sections under fire 44

Figure 3.10 Test data on (a) excess pore pressure, data extracted from (Ghaaowd et al., 2017) and (b) secant elastic modulus of clay, data extracted from (Cekerevac and Laloui, 2004).. 45
Figure 3.11 Time-dependent (a) excess pore pressure and (b) elastic modulus of clay for tunnel section 2 46
Figure 3.12 Temperature distribution within the heated part of tunnel section 1 under the RABT-train fire curve..... 47
Figure 3.13 Temperature evolution within the heated part of tunnel section 1 under the RWS fire curve 50
Figure 3.14 Comparison of vertical crown displacement for tunnel section 2 considering constant soil properties (original solution) and temperature-dependent soil properties (lower and upper bounds) 52
Figure 4.1 Damage assessment framework for RC tunnel linings exposed to fire 55
Figure 4.2 Proposed repair requirement for damage classes 61
Figure 4.3 Heated area and thermocouple locations in the test slabs 62
Figure 4.4 Temperature-time protocol for the fire tests 63

List of Tables

Table 2.1 Distribution of articles based on aggregate type 16
Table 3.1 Section and soil types of the representative four tunnel sections 33
Table 3.2 Summary of the results for the four tunnel sections under the RABT-train fire curve 48
Table 3.3 Summary of the tunnel fire performances under a 100-hour RWS fire..... 51
Table 4.1 Fire damage classification adopted from the Concrete Society (2008) 59
Table 4.2 Repair classification adopted from the Concrete Society (2008)..... 59
Table 4.3 Proposed fire damage classification as related to the results of advanced modeling 60
Table 4.4 Parameters of the fire tests 63
Table 4.5 Summary of damage assessment using a combination of observations and modeling and recommended repair strategies 65

CHAPTER 1 INTRODUCTION

1.1 Motivation

Fire is a major societal hazard with the potential to disrupt major infrastructure systems and drain valuable resources from the community. Extreme fire events, such as the 1999 Mont Blanc Tunnel fire can lead to fatalities and significant damage. In 2016 in the U.S., 475,500 structure fires caused 2,950 deaths and 7.9 billion dollars in direct property damage (Haynes, 2017). The dollar cost of structure fires increases significantly when accounting for indirect losses and expenditures, with estimates at around 1% of GDP in developed countries (CTIF, 2016; Zhuang et al., 2017). Tunnel structures with reinforced concrete liner typically behave well at high temperatures and do not collapse when subjected to moderate fires. The superior performance of concrete liners under fire, compared to other materials, relates to the low thermal conductivity of the material and the large mass of the structural components. Yet, these structures experience damage and require repair after the fire to resume function.

The available guidelines on damage assessment of concrete structures after a fire are limited (NCMA, 1994; Concrete Society, 2008; fib, 2008; ACI, 2013; ACI, 2016), and the evaluation is performed mostly on an ad hoc basis. Post-fire damage and repair classifications in the current guidelines rely on visual inspection, non-destructive testing (NDT), and sampling of material for laboratory testing. Visual inspection provides recordings of concrete color, concrete spalling, cracking, surface crazing, distortion, and deflections. Visual inspections serve as the most direct assessment, but numerous NDT techniques such as the rebound (Schmidt hammer) test and the ultrasonic pulse velocity test are used to provide a more reliable evaluation of damage. Samples of damaged material, together with undamaged benchmarks, may be removed for laboratory investigation. Concrete core samples can be taken for compression tests and petrographic examination to evaluate the depth of microcracking, paste alteration, and carbonation.

The information from visual inspections and NDT techniques can be supplemented with results of advanced modeling and analysis of the structure subjected to fire to guide the damage assessment procedure, as shown in Figure 1.1. Defining quantitative performance measures (e.g.,

temperatures reached within the cross section), and the associated damage thresholds will enable a systematic assessment of damage and a science-driven decision-making process for repair actions. Provided that information on the fire scenario can be collected to simulate the temperature-time evolution of fire during the event, the response of the structure can be evaluated and compared with the associated performance metrics.

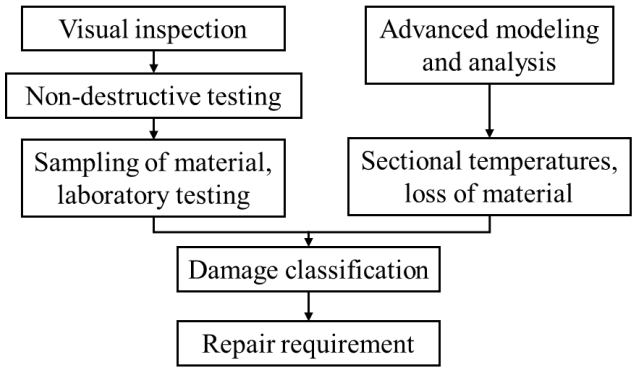

Figure 1.1 General procedure for fire damage assessment

1.2 Objective and scope

The objective of this report is to study post-fire damage assessment of reinforced concrete tunnel liners and provide recommendations on damage assessment procedures for application in practice. Post-fire assessment of reinforced concrete structures is needed to guide repair actions and ensure safety, minimize downtime, and reduce economic losses incurred due to the downtime of critical infrastructure. The outcomes of this project can be used to (1) assess the degree of in-situ damage to reinforced concrete structures affected by fire, and (2) guide performance-based fire design and assessment of reinforced concrete structures based on resilience requirements.

The report is organized in 5 chapters:

Chapter 2 “Post fire residual strength of concrete” collects experimental data on residual strength of concrete subjected to high temperatures, studies attributes that could affect the dispersion in residual strength, and proposes probabilistic models to quantify the scatter in existing data.

Chapter 3 “Influence of soil conditions on damage to tunnel structures after fire” compares the fire performance of TBM reinforced concrete tunnel lining sections in four different ground conditions, ranging from shallow-soft soil to deep-rock. The evaluation of fire performance includes the residual structural deformation and the fire resistance time. A simplified method for considering soil properties under elevated temperatures is proposed and implemented in the thermo-mechanical models.

Chapter 4 “Damage assessment” introduces a fire damage assessment framework for reinforced concrete tunnel linings, which integrates advanced modeling with visual inspections, non-destructive testing, and material sampling. A damage classification system based on a collection of international guidelines and feedback from industry experts is discussed to systemically define and map damage metrics and repair strategies. A case study, using data from recent experiments, is conducted to demonstrate the applicability of the proposed framework.

Chapter 5 “Conclusions and recommendations” provides a summary of research findings, conclusions, and recommendations.

CHAPTER 2 POST-FIRE RESIDUAL STRENGTH OF CONCRETE

There is a relatively large number of experimental studies on the residual compressive strength of concrete after exposure to high temperatures. However, estimating the residual strength of concrete remains a challenge due to the large scatter in the data. The large variability in existing datasets is related to the inherent uncertainty in the material behavior in addition to variations in various attributes of the experiments, e.g., a lack of consistency in testing protocols.

The objective of this chapter is to provide a comprehensive review of experimental investigations on the residual compressive strength of concrete after exposure to high temperatures. The existing data are analyzed to identify attributes that could affect the dispersion in residual strength, such as the aggregate type, concrete mix, and testing protocol. Categories with limited data points that require further research are identified. The refined datasets are then used to develop probabilistic models for the normalized residual compressive strength of concrete. The proposed models have simple mathematical forms that can be applied in analytical and computational frameworks. Both data and proposed models are compared with the Eurocode 2 (EC2) (CEN, 2004) prescribed values for the residual strength of concrete after fire and the suitability of the EC2 reduction factors is discussed.

2.1 Methodology

The content analysis approach proposed by Mayring (2004) is applied to collect and review the available literature on residual compressive strength of concrete after exposure to high temperatures. The review is carried out systematically, following a four-step process:

1. Material collection: comprises a well-organized search and delimitation of articles.
2. Descriptive analysis: identifies the general features of the literature under review.

3. Category selection: builds a categorization framework based on relevant dimensions. For this study, attributes of the data that could influence the outcome are identified.
4. Material evaluation: reviews and interprets articles using the given categorization framework.

The first three steps are discussed in the following subsections. The final step is explored in greater detail along with the analysis of collected data on the residual compressive strength of concrete.

2.1.1 Material collection

The following criteria were considered when conducting the literature review: (1) papers that provided experimental data on the residual compressive strength of concrete subjected to high temperatures were collected, (2) papers that included experimental data on compressive strength of concrete at high temperatures (i.e., measurements done while specimens were hot) were excluded, and (3) published journals papers for a time span of 30 years (from 1990 to 2020) were included. Considering these criteria, a total of 60 articles containing 1400 data points on the residual compressive strength of concrete as a function of temperature were identified. Further, only the data points for concrete with a compressive strength of less than 55 MPa at room temperature, i.e., normal strength concrete (NSC), were kept in the dataset. Thus, 53 articles with a total of 1240 (out of 1400) data points were selected for review and analysis.

2.1.2 Description analysis

The distribution of specimen types in the examined literature is shown in Figure 2.1. There is a relatively uniform distribution between cube versus cylinder specimens. In most of the European studies, the compressive strength is measured using cubic specimens, whereas cylinders are used in the United States and Australia. Pacheco et al. (2019) proposed a cube to cylinder conversion factor of 0.81 for normal aggregates and 0.77 for recycled aggregates. The conversion factors were applied to cubic samples before grouping the data based on concrete strength (normal vs. high strength).

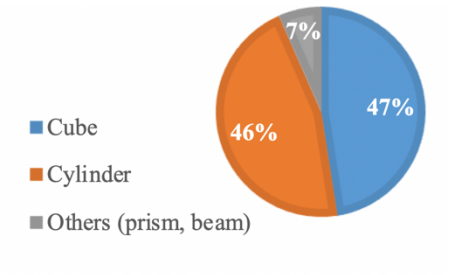

Figure 2.1 Distribution of specimen type in the collected data

2.1.3 Category selection

The collected literature included variations in a series of attributes, including the aggregate type, concrete mix, and testing protocol, when investigating the residual compressive strength of concrete as a function of temperature. These attributes are listed in Figure 2.2 and their influence on the residual strength of concrete is studied in this chapter.

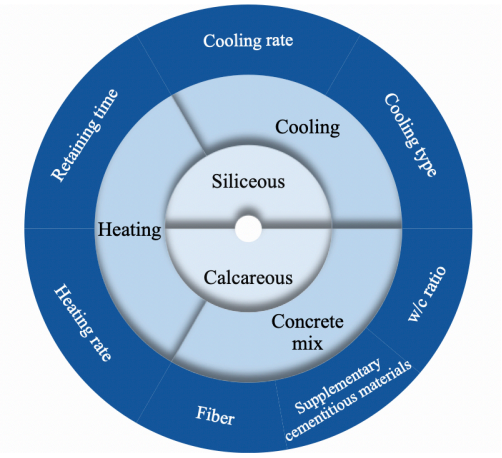

Figure 2.2 Collected parameters that could influence residual compressive strength of concrete exposed to high temperatures

About 80% of concrete is made up of coarse aggregate and the aggregate type has an effect on the residual compressive strength of concrete that is exposed to high temperatures (CEB-FIP,

2007). The most often used categories for aggregate types are siliceous and calcareous aggregates. Calcareous aggregates are sedimentary rocks that are primarily composed of calcium carbonate (CaCO3), such as limestone or dolomite, whereas siliceous aggregates are mainly composed of silica (SiO2, i.e., combination of silicon and oxygen) and silicates (combination of silicon, oxygen, and other elements). Thermal incompatibility between the aggregate and cement paste causes degradation in mechanical properties of concrete at high temperatures. The higher the aggregate's coefficient of thermal expansion, the more damage the concrete experiences when exposed to high temperatures (CEN, 2004).

The rest of the considered parameters are related to the concrete mix and testing protocol. Concrete mix includes the water/cement (w/c) ratio and inclusion of any fibers and/or supplementary cementitious materials (SCM). The testing protocol refers to the heating rate, retaining time, cooling rate, and cooling method (e.g., air or water).

2.2 Material evaluation

The following sections will categorize and analyze the dataset to identify parameters that influence the residual compressive strength of concrete. These parameters are used to define sub-groups within the dataset that perform similarly and exhibit less scatter. Observations from collected data are also compared with reduction factors from EC2 (CEN, 2004) to assess the suitability of prescribed values by the code. Finally, analysis of data is used to identify areas that require further investigation.

2.2.1 Effect of course aggregate

The selection and characterization of the coarse aggregate likely has the most influence on the performance of concrete at high temperatures (Sollero et al., 2021). Siliceous and calcareous aggregates are the two major coarse aggregate types utilized in concrete mixtures. EC2 specifies the loss in concrete strength due to temperature based on the type of coarse aggregate. EC2 further provides reduction factors for concrete compressive strength at high temperatures and prescribes an additional 10% reduction to determine the residual strength after exposure to high

temperatures. Table 2.1 lists the collected articles in this research based on the aggregate type in tested specimens. The collected dataset, targeting publications post 1990, includes 1240 data points with a substantial percentage focusing on siliceous aggregate, accounting for roughly 87% of the dataset.

Table 2.1 Distribution of articles based on aggregate type

Aggregate type	References
Siliceous	Sullivan and Sharshar 1992; Chan et al. 1999; Luo et al. 2000; Zhang et al. 2000; Barragán et al. 2001; Poon et al. 2001; Tolentino et al. 2002; Poon et al. 2003; Li et al. 2004; Abramowicz and Kowalski 2005; Sakr and El-Hakim 2005; Chang et al. 2006; Lau and Anson 2006; Zega and Di Maio 2006; Arioz 2007*; Lee et al. 2008; Sancak et al. 2008; Anagnostopoulos et al. 2009; Bingöl and Gül 2009; Chen et al. 2009; Tang and Lo 2009; Demirel and Keleştemur 2010; Tanyildizi and Çevik 2010; Esen 2010; Rama Seshu and Pratusha 2013; Sarhat and Sherwood 2013*; Xiao et al. 2013; Chen et al. 2014*; Mathew and Paul 2014; Al-Jabri et al. 2016; Bideci 2016; Martins et al. 2016; Torić et al. 2016; Yaqub and Bailey 2016; Tufail et al. 2017*; Türkmen et al. 2017; Bui et al. 2018; Xie et al. 2018; Yang et al. 2018; Ren et al. 2019; Salahuddin et al. 2019; Khan et al. 2020; Sachin and Suresh 2020; Yonggui et al. 2020; Zhao et al. 2020
Calcareous	Phan et al. 2001; Anwar Hossain 2006; Arioz 2007*; Arioz 2009; Ghandehari et al. 2010; Sarhat and Sherwood 2013*; Ahmad et al. 2014; Chen et al. 2014*; Tufail et al. 2017*; Rafi et al. 2018; Varona et al. 2018; Eidan et al. 2019

*Four articles investigated both calcareous and siliceous aggregates.

Figure 2.3 presents the normalized residual compressive strength of concrete as a function of temperature and based on aggregate type. The residual compressive strength data (f'_c) were normalized using the average of values recorded at room temperature ($f'_{c,20}$). The plots include EC2 reduction factors (EC_Si and EC_Ca) for comparison with data. The normalized residual compressive strength for both aggregate types show large variations across different temperatures. The figures also include box plots, indicating the first quartile (Q1), third quartile (Q3), median, whiskers that span 1.5 times of the inter-quartile range, and the outliers. The median of the data for siliceous aggregate is slightly higher than the EC2 values (EC_Si), whereas

in the case of calcareous aggregate, the median of data falls below the EC2 (EC_Ca) reduction factors, noting that there is a smaller number of data points available compared to the siliceous category.

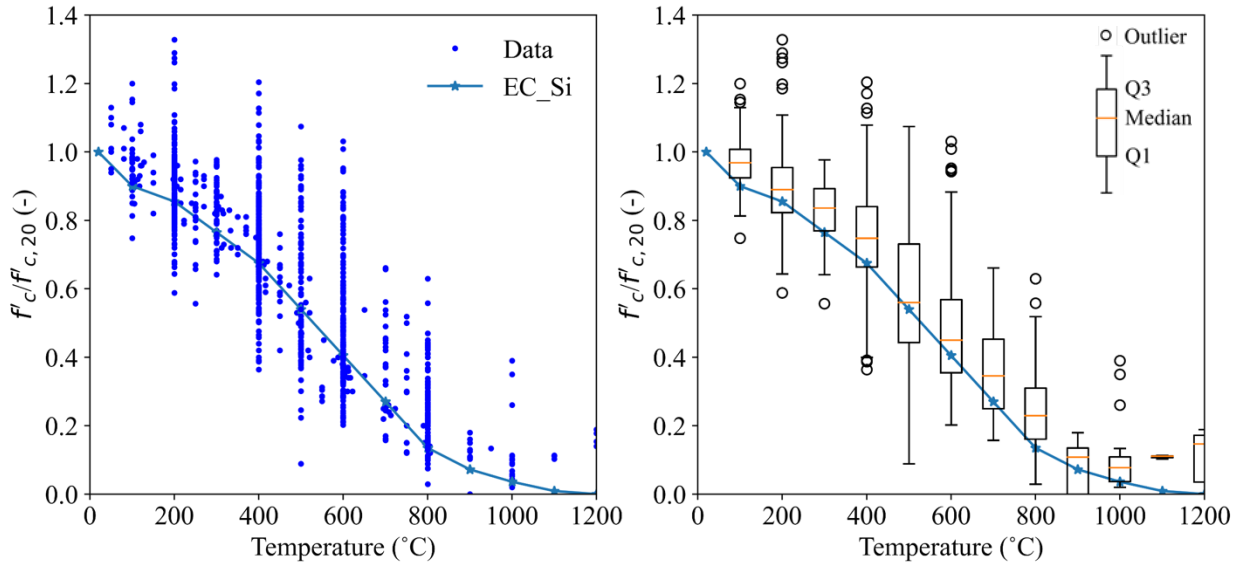

(a)

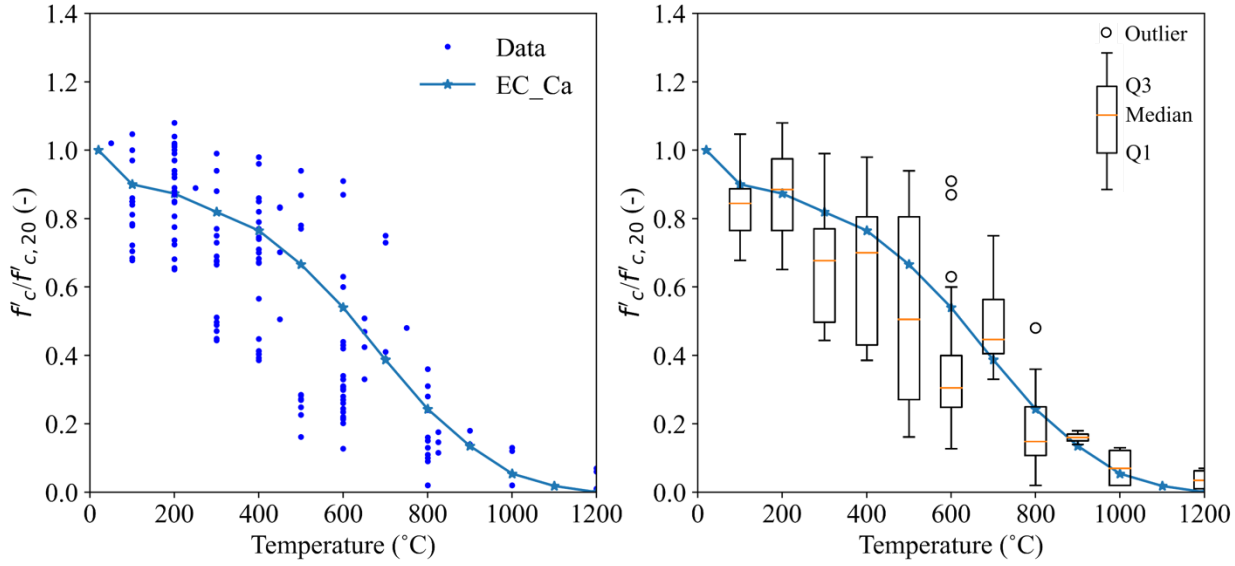

(b)

Figure 2.3 Normalized residual strength of concrete as a function of temperature for experimental data and the Eurocode 2 reduction factors for (a) siliceous and (b) calcareous aggregate types

2.2.2 Effect of testing protocol

Nassif (2006) argued that knowing the maximum exposure temperature is insufficient for estimating the postfire strength of concrete; however, no standard testing protocol exists for evaluating the effects of high temperatures on concrete, resulting in variations in conducted experiments in the literature and the potential for a large scatter in the published results (Deshpande et al., 2019). The testing protocol includes the rate of heating, maximum temperature, retaining time, rate of cooling, and type of cooling. The maximum temperature for the test is typically varied to obtain reduction factors as a function of temperature. Thus, the heating rate and the retaining time are the two main variables for the heating protocol.

The heating rate is the rate at which the furnace temperature rises over time. A rapid heating rate decreases the time it takes to reach the required temperature inside a furnace, but it can lead to considerable temperature variations inside concrete specimens (Kumar and Ranade, 2021). Sachin (2020) studied the effect of heating rate using gas and electric furnaces, and concluded that fire-exposed specimens had lower residual compressive strength than specimens heated in an electric furnace at the same temperature. Gas furnaces typically follow the standard fire curve (ASTM E119 or ISO834) whereas electric furnaces have a lower heating rate compared to standard fire curves. Although the compressive strength of concrete appears to be affected by different heating rates, the majority of the reviewed articles used an electric furnace due to the safety requirements and expenses of a gas furnace. Figure 2.4 groups the data based on heating rate, demonstrating that limited data is available with the standard fire curve as the heating protocol.

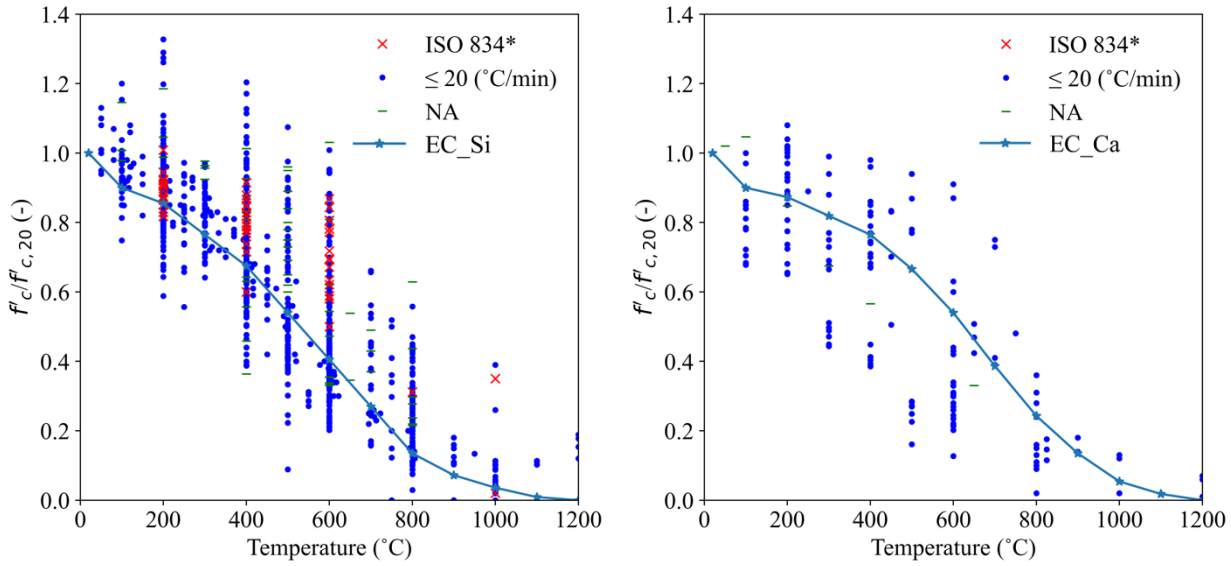

Figure 2.4 Normalized residual strength of concrete with (a) siliceous and (b) calcareous aggregates categorized based on different heating rate (*or ASTM E119)

Zega (2006), Sakr and Hakim (2005), and Zhang (2000) studied the effect of retaining time on the residual strength of concrete with siliceous aggregate, as the core temperature of a concrete specimen lags behind the surface temperature due to the low thermal diffusivity of concrete. The retaining time (t_R) is the duration that a specified furnace temperature is maintained once it has been reached. In general, longer exposure times ensure a greater volume of a specimen reaches thermal equilibrium with the furnace environment, which has a considerable impact on residual compressive strength (Deshpande et al., 2020). Figures 2.5 and 2.6 group the normalized residual compressive strength data based on the retaining time of less than and larger than 2 hours for silicious and calcareous aggregates, respectively. Figure 2.5 shows that introducing the retaining time to categorize the experimental data reduces the scatter in data for siliceous aggregate, especially in the range of 400 – 700°C. In Figure 2.5, the medians of the box plots for data with a retaining time greater than 2 hours are better matched with the EC2 reduction factors, whereas the medians of box plots for retaining time less than 2 hours fall above the EC2 reduction factors.

Comparing the two categorizes emphasizes the need to allow sufficient time for the heat to reach the specimens' cores to obtain proper measurements. After investigating multiple thresholds on the dataset, the minimum two hours of retaining time was found to be necessary for lowering the standard deviation of normalized concrete strength. Figure 2.6 plots similar data but for concrete with calcareous aggregates. It is shown that data with retaining times greater than 2 hours fall below the EC2 reduction factors, whereas those with less than 2 hours of retaining time match better with Eurocode2. This implies that the EC2 reduction factors may not be conservative for concrete with calcareous aggregates. Overall, more data is needed for concrete with calcareous aggregates to confirm the conclusions.

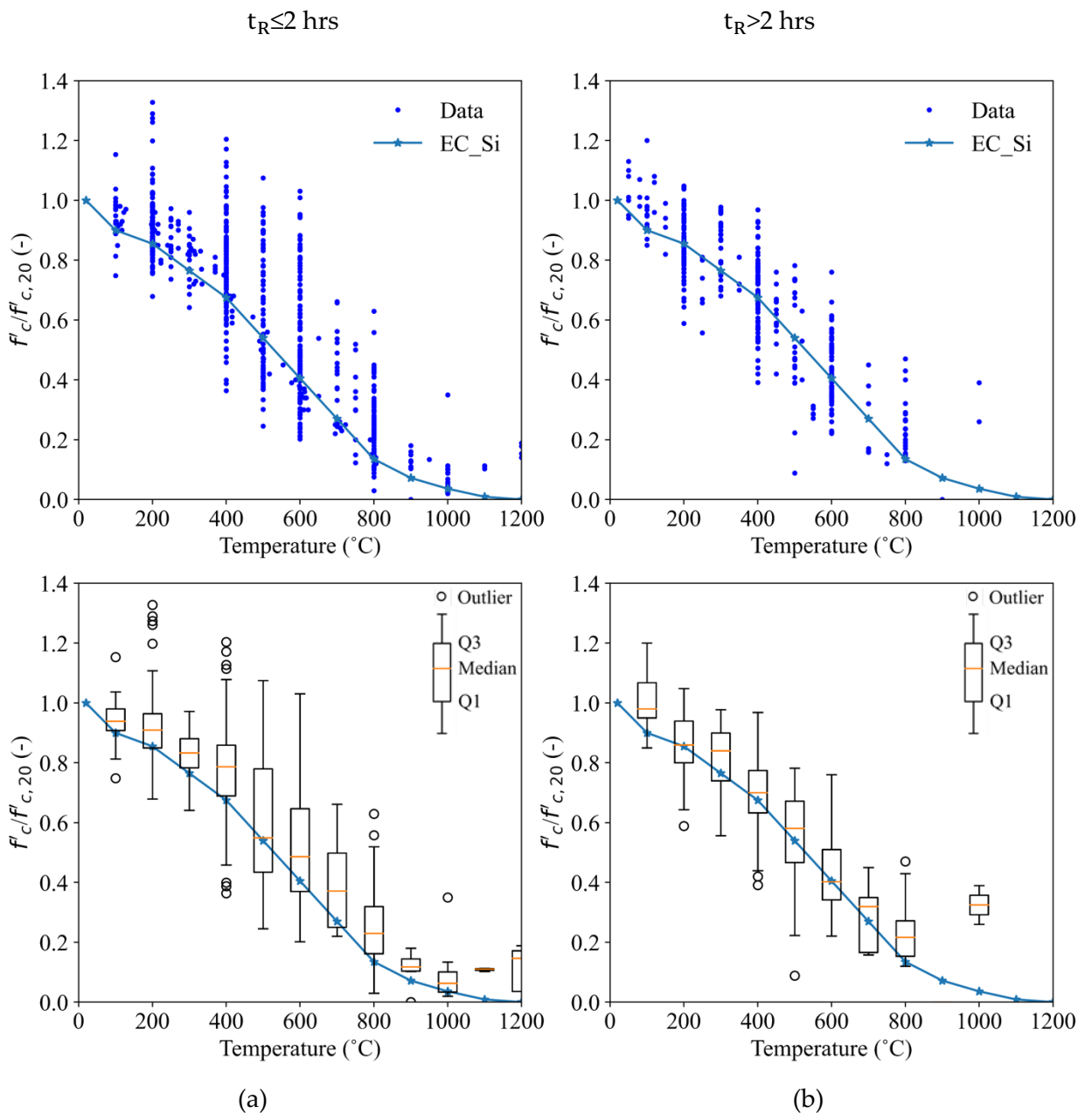

Figure 2.5 Normalized residual compressive strength of concrete with siliceous aggregate and retaining time (a) less than or equal to 2 hours, (b) greater than to 2 hours

$t_R \leq 2$ hr. $t_R > 2$ hr.

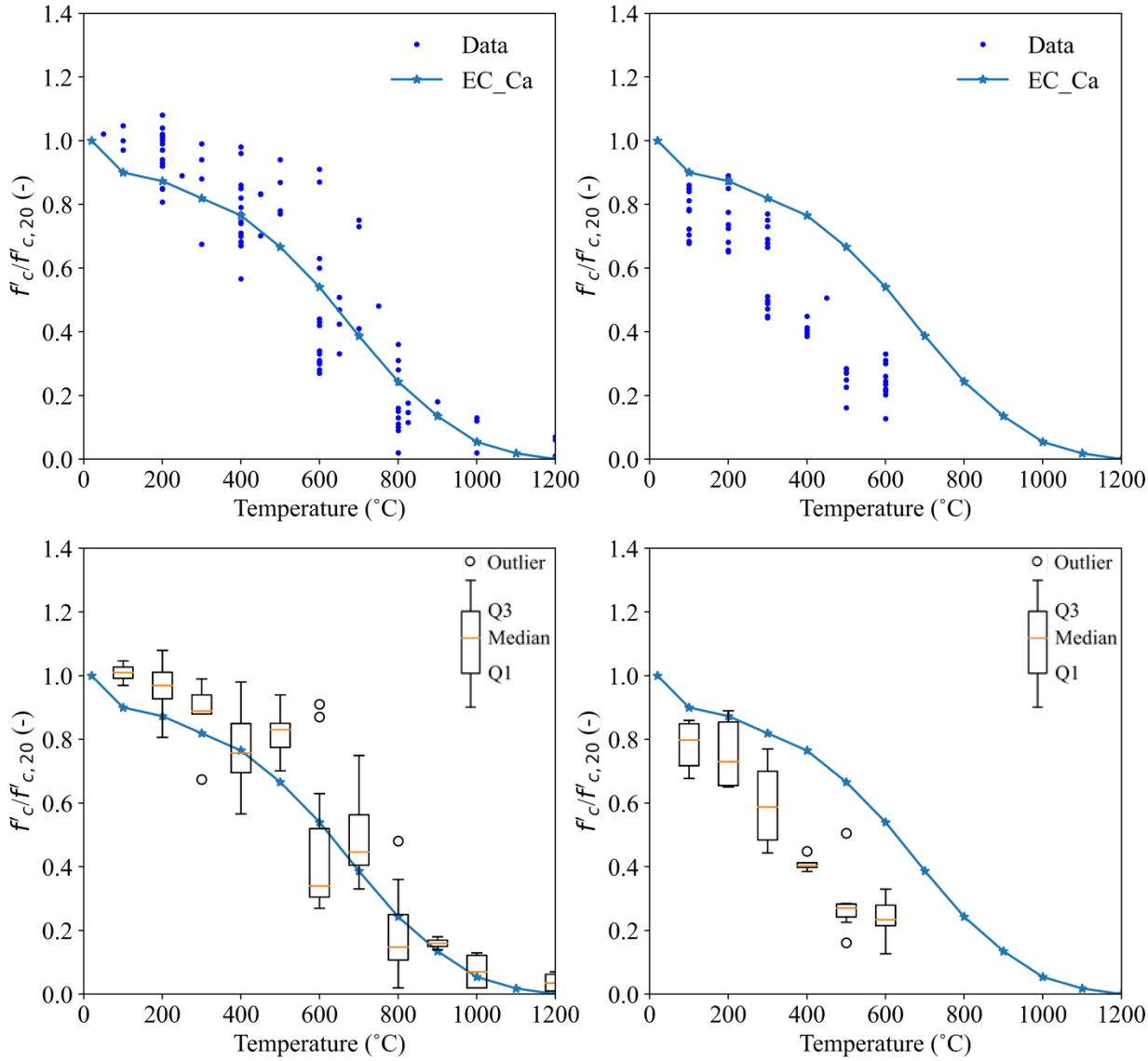

Figure 2.6 Normalized residual strength of concrete with calcareous aggregate and retaining time (a) less than or equal to 2 hours, (b) greater than to 2 hours

2.3 Probabilistic model for post-fire residual strength of concrete

This section will discuss and develop a probabilistic model for the residual compressive strength of concrete after exposure to high temperatures (i.e., post-fire) based on the collected and refined dataset in the previous sections. Qureshi et al. (2020) quantified uncertainties in retained strengths of steel and concrete at high temperatures (i.e., during fire). Different distribution candidates were used with the collected data to identify the most suitable probabilistic model. In addition, the models were considered to be continuous functions that could be implemented in analytical and computational frameworks. A similar approach by Qureshi et al. (2020) is used in this section to propose probabilistic models for post-fire residual compressive strength of concrete.

2.3.1 Evaluate candidate distributions

A total of 401 and 159 data points, collected from the literature, were used to develop the probabilistic models for residual compressive strength of normal strength concrete containing siliceous and calcareous aggregates, respectively. As stated previously, the data points for concrete with siliceous aggregate are filtered to have a retaining time of more than 2 hours to remove some of the large dispersions at certain temperature intervals. Raw data were then grouped at temperature intervals of 50°C to capture variability in data at distinct temperature intervals. Each temperature group comprised data points within a ±10°C range, and datasets containing less than 5 data points were discarded. Consequently, 11 temperature groups for siliceous aggregate concrete and 7 temperature groups for calcareous aggregate concrete were created. Figure 2.7 shows the raw data with dashed lines indicating the selected temperature groups, which will be used in the next step to develop the probabilistic models. The groups range between 50°C and 800°C. Noting that the data is normalized using the average measured value of concrete compressive strength at 20°C; therefore, the variability of data at ambient temperature is minimal. To capture the scatter in concrete compressive strength at room temperature, and for consistency with existing models for ambient design, a mean value of 1.0 with a coefficient of variation (COV) of 0.12 is imposed at 20°C when developing the probabilistic models. The

selected value of the COV is based on the recommendation by Holický and Sýkora (2010) for normal strength concrete compressive strength at 20°C.

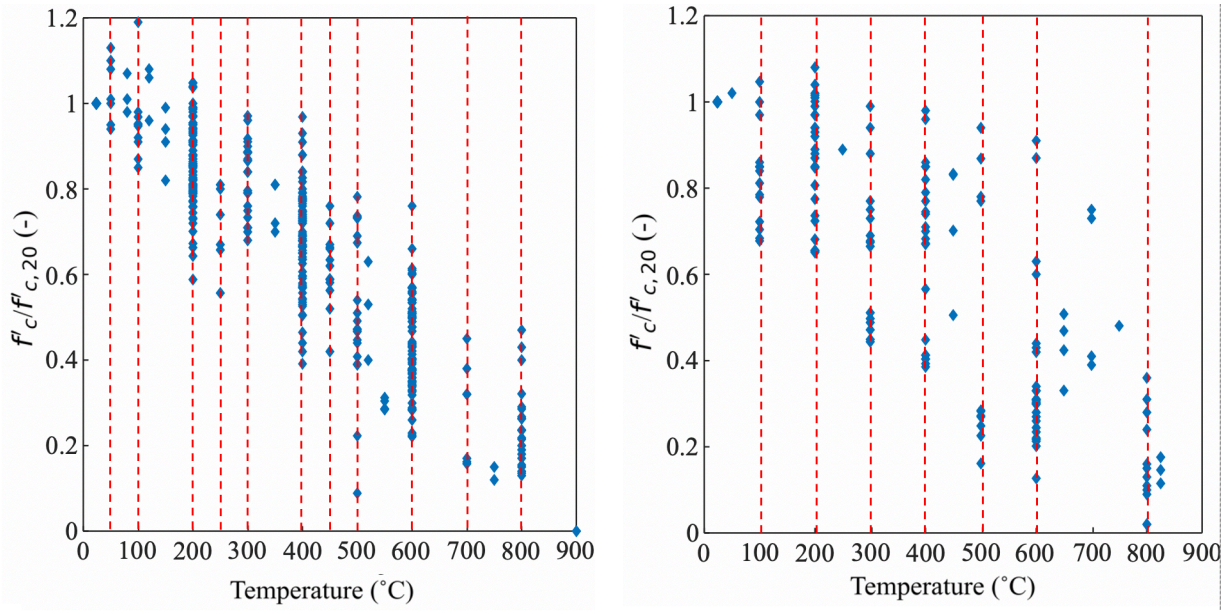

(a) (b)

Figure 2.7 Grouped data points for concrete with (a) siliceous (b) calcareous aggregates

In the next step, 13 distinct probability density functions (PDF) were chosen as competing models, and their quality was assessed to select the best candidate. The selected functions that were fit to the data groups at each specific temperature are the: gamma, normal, lognormal, logistic, loglogistic, inverse Gaussian, Gumbel, generalized t-distributions, beta44, Rician, Nakagami, Bimbaum-Saunders, and Weibull. To compare the distributions, three information criteria were used to quantify the relative goodness of each fit across all temperature groups, namely: (1) Bayesian information criterion or BIC; (2) Akaike information criterion or AIC; (3) Corrected AIC or AICc.

- The BIC calculates the maximum likelihood estimate, by adopting the negative measure of the fit as -2 × loglikelihood and penalizing complexity as a positive log(N) × k, where N is the number of samples and k is the total number of model parameters (Schwarz, 1978).

- The AIC also applies the penalized likelihood criterion, but instead of log(N), it weighs k with a constant value of 2 (Akaike, 1974).
- The AICc is equal to AIC + $\frac{2k^2+2k}{N-k-1}$, introducing an adjustment by the inclusion of an additional penalty for small-sized datasets (Hurvich and Tsai, 1993).

The three listed criteria were first computed at every temperature group for each of the 13 candidate distributions. Then, the mean across all the temperature groups was evaluated for each of the three criteria. Each bar in Figure 2.8 represents the mean value for the three information criteria and all candidate distributions. A model with a lower BIC, AIC, or AICc value is considered to be of higher quality. The concrete data with calcareous aggregates had a small number of datapoints, for which the AIC may overfit whereas the BIC may underfit. Therefore, the AICc is a more suitable criterion to identify models with a better fit.

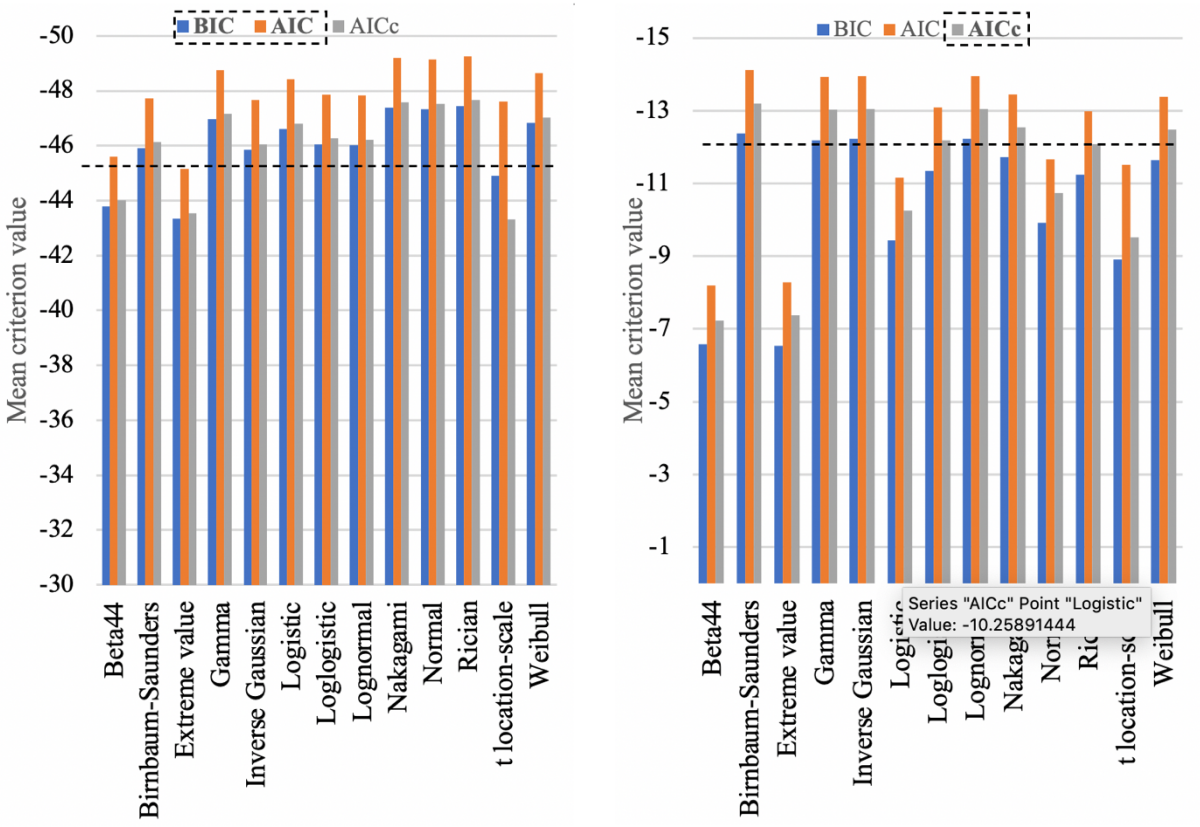

(a) (b)

Figure 2.8 Comparison of the mean criterion value for each of the 13 candidate PDF models for the residual compressive strength of concrete with (a) siliceous (401 points) and (b) calcareous (159 points) aggregates

Figure 2.8 shows that several distributions perform relatively better than the others considering both siliceous and calcareous datasets: gamma, inverse Gaussian, lognormal, Nakagami, and Weibull. A few additional requirements are imposed to select the final stochastic functions:

- The chosen models should be a "continuous function" that appropriately captures scatter within experimental data for material strengths ranging from 20°C to 1000°C.
- There should be a "closed-form function" available for presenting quantiles of the model in order to facilitate implementation in analytical and computational frameworks.

On the basis of these additional requirements, the selected models were narrowed down to two distribution models: Weibull and lognormal. Figure 2.9 shows the PDF for the Weibull and lognormal models against data for 200°C, 300 °C, and 400 °C. Both distributions could represent the data; however, the Weibull function was chosen for both aggregate types moving forward. This ensures compatibility with established stochastic functions for concrete strength at high temperatures by Qureshi et al. (2020) and prevents potential confusion in use the of the models in future.

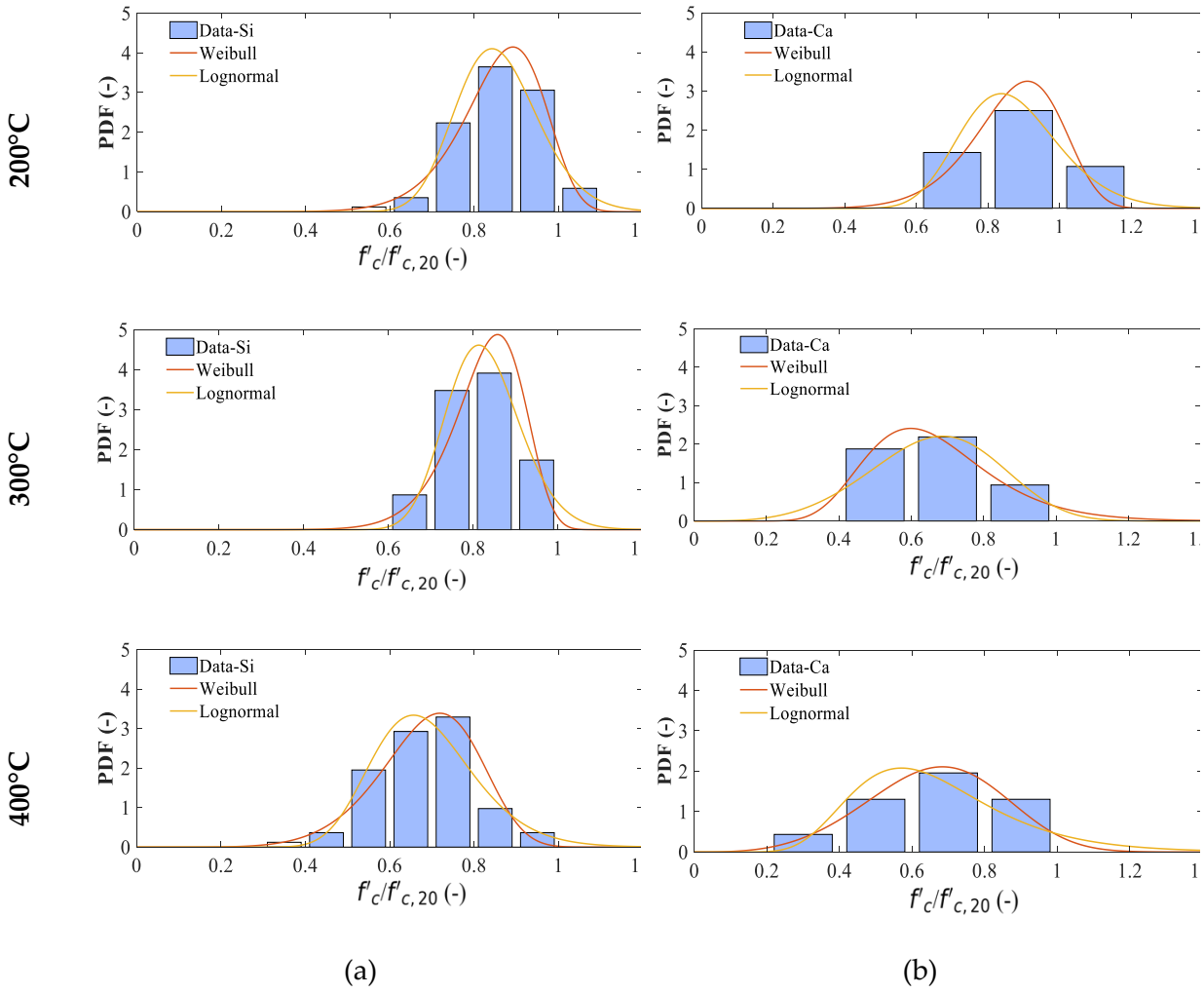

Figure 2.9 Selected probabilistic models along with PDF for normalized residual strength for (a) siliceous and (b) calcareous concrete data at 200°C, 300°C, and 400°C

2.3.2 Temperature-dependent parameters of the Weibull distribution

The Weibull distribution is a PDF with two variables: scale (λ) and shape (k) parameters, as defined below:

$$f(x;\lambda,k) = \begin{cases} \frac{k}{\lambda}\left(\frac{x}{\lambda}\right)^{k-1} e^{-\left(\frac{x}{\lambda}\right)^{k}}, & x \geq 0 \\ 0, & x < 0 \end{cases} \tag{2.1}$$

The two parameters of the Weibull distribution were determined for each temperature group of the concrete data with siliceous and calcareous aggregates, as presented in Figure 2.10. Nineteen alternative polynomial functions were selected to fit to the parameters as a function of temperature. The R-squared value was calculated for each polynomial fit and used to assess how well the data matched the regression function. A larger R-squared value implies that the polynomial function provides a better match with the data. Aside from the R-squared value, a few other factors were considered to select the function with the best estimate. For example, the scale parameter (λ) should have a decreasing trend for the temperature range of 20 to 1000°C, and the shape parameter (k) should be greater than 1. The red lines in Figure 2.10 are the best fit polynomial regressions for the scale and shape parameters of the Weibull distributions for the residual strength of siliceous and calcareous concretes. The following are the corresponding equations for the temperature-dependent parameters of the Weibull distribution for siliceous concrete:

$$\lambda(T) = 1.06 \times 10^{-3}T + 1.11 \tag{2.2}$$

$$k(T) = \frac{95.27}{5.095 + 23.21 \times 10^{-3}T} \tag{2.3}$$

Similarly, temperature-dependent parameters of the Weibull distribution for calcareous concrete can be determined using the following equations:

$$\lambda(T) = 1.06 \times 10^{-3}T + 1.068 \tag{2.4}$$

$$k(T) = \frac{18.92}{1.617 + 8.38 \times 10^{-3}T} \tag{2.5}$$

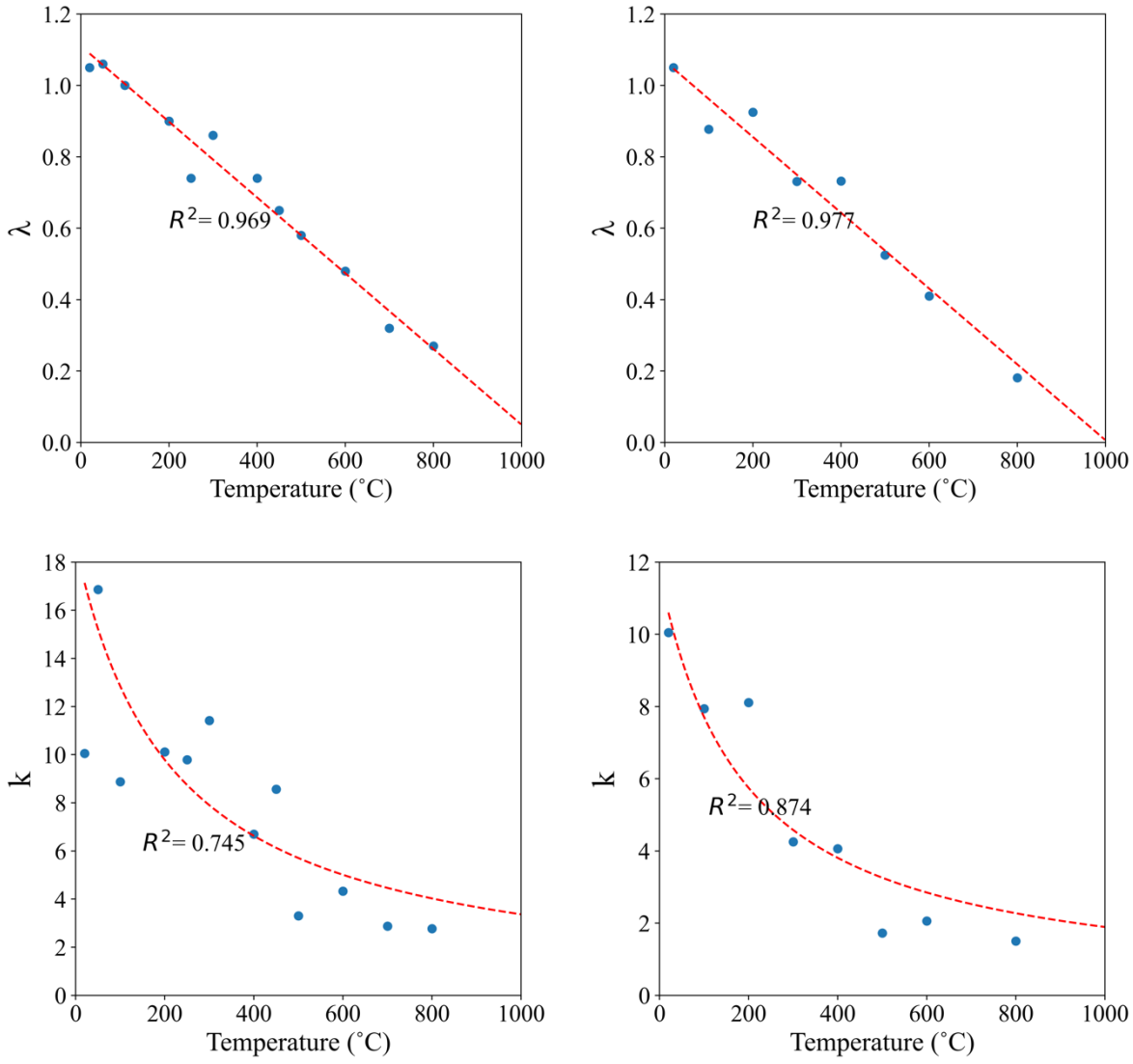

(a) (b)

Figure 2.10 Temperature-dependent polynomial regression for λ and *k* representing (a) siliceous concrete and (b) calcareous concrete

The temperature-dependent polynomial equations for λ and *k* are used with the Weibull distribution function to plot the 0.5, 0.05, and 0.95 quantiles as shown Figure 2.11. The EC2 reduction factors and experimental data from literature are also shown in the figure. It can be seen that the EC2 reduction factors are relatively close to the median of the Weibull distribution for siliceous concrete, and the model captures the uncertainty in collected data from the literature.

For calcareous concrete, the median of the Weibull distribution is lower than the EC2 reduction factors. If a refined dataset with a retaining time greater than 2 hours were used to develop the probabilistic model, the median would have been even lower. Thus, it appears that the EC2 model tends to overestimate the residual compressive strength of concrete with calcareous aggregate.

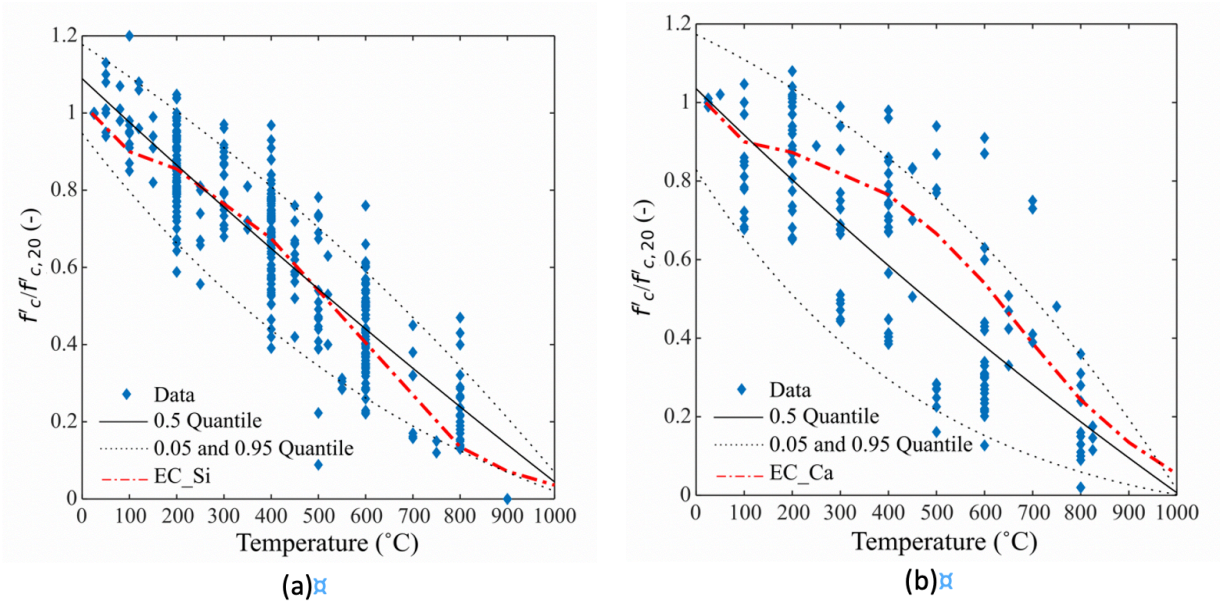

Figure 2.11 Temperature-dependent residual strength data for normal strength concrete versus the Weibull probabilistic model and EC2 reduction factors for: (a) siliceous concrete, and (b) calcareous concrete

2.4 Conclusion

This chapter collected and analyzed experimental data on the residual compressive strength of normal-strength concrete after exposure to high temperatures. A total of 53 papers, published after 1990, were reviewed and 1240 datapoints on the residual compressive strength of concrete as a function of temperature were collected. The dataset was first analyzed to identify attributes that could affect the residual strength of concrete. The refined dataset was then utilized to propose a probabilistic model for the residual compressive strength of concrete to capture the uncertainties in material strength as a function of the maximum exposure temperature. Conclusions of this chapter can be summarized as below:

- In the collected database, only 159 datapoints (of the 1240) studied concrete with calcareous aggregates. Thus, the majority of existing research has focused on siliceous concrete with limited data available for calcareous concrete.
- There is no standard testing protocol to evaluate degradation of mechanical properties of concrete at high temperatures. Thus, the employed testing protocol in existing experiments varied. Analyses of data showed that the duration of the retaining time at the maximum temperature had a significant influence on the scatter of the data. The specimen should be heated for enough time so that the core reaches the target temperature. Based on the results of this study, a minimum retaining time of 2 hours is recommended to ensure uniform temperature in the specimen. Overall, there is a need to research a standard testing protocol that defines acceptable heating rates, retaining times, and cooling rates.
- Probabilistic models utilizing Weibull distributions were established to quantify uncertainties in the temperature-dependent residual compressive strength of siliceous and calcareous concrete. The parameters of the Weibull distributions were defined as continuous closed-form solutions as a function of temperature.

The medians of data and proposed probabilistic model for the siliceous concrete are close to the EC2 model. However, the EC2 model tends to overestimate the reduction factors for calcareous concrete when compared with the medians of the data and the proposed model.

CHAPTER 3 INFLUENCE OF SOIL CONDITIONS ON DAMAGE TO TUNNEL STRUCTURES AFTER FIRE

The fire behavior of a tunnel lining structure is influenced by a series of parameters, including fire temperature and duration, type of lining material (e.g., fiber-mixed concrete vs. conventional concrete), surrounding soil conditions (e.g., soft soil vs. rock), level of water table, etc. Hence, the structural performance under fire can vary significantly from tunnel to tunnel as well as from section to section in the same tunnel. Moreover, modern tunnels tend to use thinner reinforced concrete (RC) sections. As a result, the local soils or rock may also be heated through heat transfer within the lining section, and undergo a coupled thermo-hydro-mechanical process during fire, which in turn changes the level of constraint to the tunnel structure. The combined influence of the aforementioned parameters creates significant complexities in analyzing the fire behavior of tunnel structures.

This chapter seeks to compare the fire behavior of four bored RC tunnel sections under different geologic conditions through a series of thermo-mechanical analyses. The analyses are conducted using the finite-element software program SAFIR (Franssen and Gernay, 2017) and the modeling method has been verified. The four ground conditions are obtained from high-profile TBM (tunnel boring machine) excavated tunnels, and the RC sections are designed based on the latest codes and guidelines. The results are organized in the following three categories: (1) the fire behavior of four tunnel sections under the RABT-train fire curve is simulated for 72 hours to compare their structural performance during heating, cooling and after fire; (2) the four tunnel sections are subjected to an extended RWS fire to quantify the failure time of the tunnel sections; (3) a preliminary analysis is completed to investigate the heat induced excess pore pressure on the tunnel section and the change in subgrade reaction modulus under elevated temperatures, as well as their influence on the structural fire performance of a tunnel section. Note that the first two parts consider constant soil properties in the models.

3.1 Representative geologic profiles for realistic tunnel sections

The geologic profiles of four tunnel sections, ranging from shallow to deep, and with the ground conditions ranging from soft soil to rock, are selected as representative cases and listed in Table 3.1. The four sections are obtained from three high-profile tunnels: the Second Heinenoord Tunnel (shallow - soft soil) in the Netherlands (Ngan et al., 2017), the Storebælt Railway Tunnel (moderate-depth - soft soil) connecting Zealand and Denmark (BTS, 2004), and the Channel Tunnel (moderate-depth to deep - rock) located between the UK and France (BTS, 2004). The three tunnels are all TBM excavated tunnels with circular RC sections. The inner diameters of the interested tunnel sections range from 7.3 m to 7.7 m.

Table 3.1 Section and soil types of the representative four tunnel sections

	Tunnel section 1	**Tunnel section 2**	**Tunnel section 3**	**Tunnel section 4**
Section depth	Shallow (< 20m)	Moderate (20-50m)	Moderate (20-50m)	Deep (> 50m)
Soil type	Soft (sand, clay)	Soft (till)	Rock (chalk marl)	Rock (chalk marl)

3.1.2 Tunnel section 1: a shallow section in soft soil

Tunnel section 1 is adopted from a tunnel section located on the North Bank of the Second Heinenoord Tunnel in Rotterdam, the Netherlands (Ngan et al., 2017). The tunnel axis of section 1 is located at about 16.25 m below the ground surface, with an inner diameter of 7.6 m and lining thickness of 0.35 m. The description of the soil layers and parameters is shown in Figure 3.1, where H is the depth of the tunnel axis, H_w is the distance between tunnel axis and the water table, d is the soil layer thickness, γ is the unit weight, ν is the Poisson's ratio, E is the elastic modulus, and K_0 is the lateral pressure coefficient of the soil layer. As Figure 3.1 shows, the majority of the tunnel section is located within the third soil layer, which is composed of sand and clay with an elastic modulus of 40 MPa.

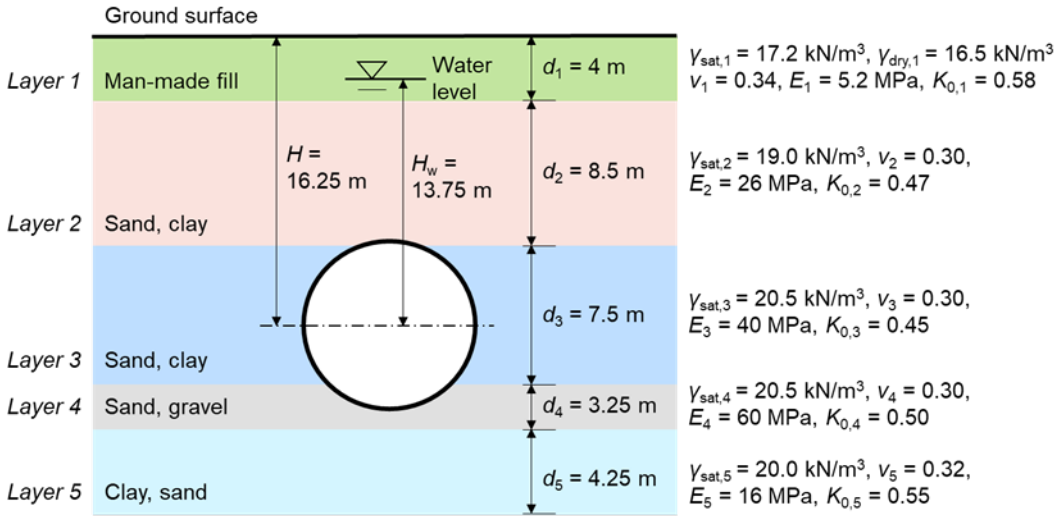

Figure 3.1 Geologic profile for tunnel section 1 (data from (Ngan et al., 2017))

3.1.3 Tunnel section 2: a moderate-depth section in soft soil

The Storebælt railway tunnel provides a link across the Eastern Channel between Zealand and the small island of Sprogø in Denmark (BTS, 2004). Tunnel section 2 is located where the tunnel axis is about 25 m below the ground surface and 31 m below the sea level, as Figure 3.2 shows. The inner diameter of the tunnel lining is 7.7 m, and its thickness is 0.4 m. The whole tunnel section is located in the till layer, with an average elastic modulus of 23 MPa.

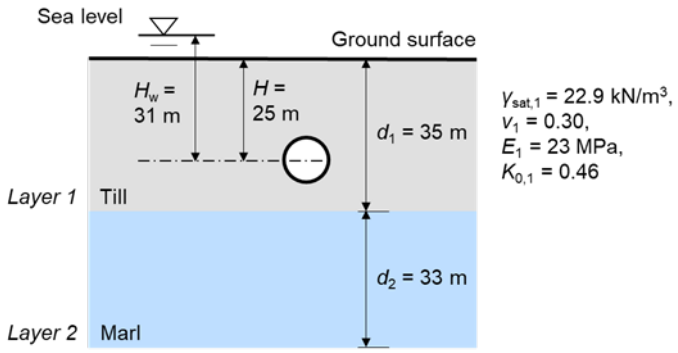

Figure 3.2 Geologic profile for tunnel section 2 (data from (BTS, 2004))

3.1.4 Tunnel section 3: a moderate-depth section in rock

The Channel Tunnel is a TBM excavated railway tunnel, with an inner diameter of 7.3 m. The majority of the Channel Tunnel is located within the chalk marl (a calcareous jointed mudstone) layer (BTS, 2004). Three major tunnel fires occurred in the Channel Tunnel in 1996, 2006, and 2008. Tunnel section 3 is located at the French side of the Channel Tunnel. Most of section 3 is in the upper chalk marl layer, which has an average elastic modulus of 1300 MPa. The soil data for tunnel section 3 is shown in Figure 3.3, note that the dimensions are approximate.

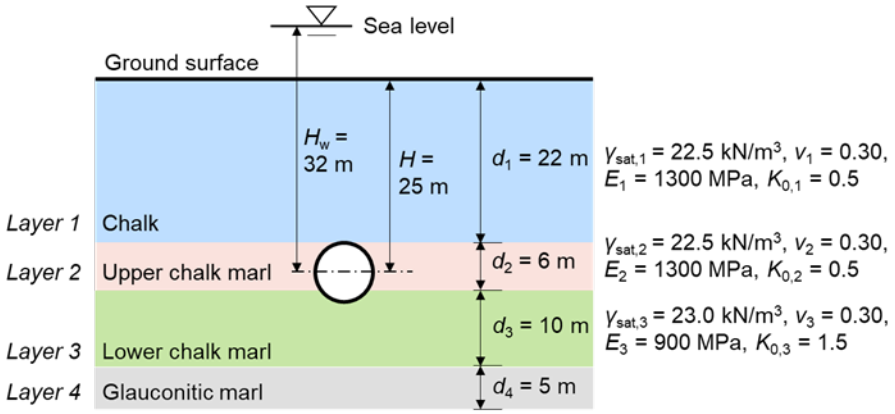

Figure 3.3 Geologic profile for tunnel section 3 (data from (BTS, 2004))

3.1.5 Tunnel section 4: a deep section in rock

Tunnel section 4 located at the UK side of the Channel Tunnel. This section is considered as a deep section with a central depth of about 162 m, due to the existence of the Shakespeare Cliff on the UK side. Tunnel section 4 is in the lower chalk marl layer, which has an average elastic modulus of 900 MPa (BTS, 2004). It is worth mentioning that the lateral pressure coefficient (K_0) of the lower chalk marl layer is 1.5, implying that tunnel section 4 would be subjected to a relatively high level of lateral soil pressure. The soil data for tunnel section 4 is shown in Figure 3.4, where the dimensions are approximate.

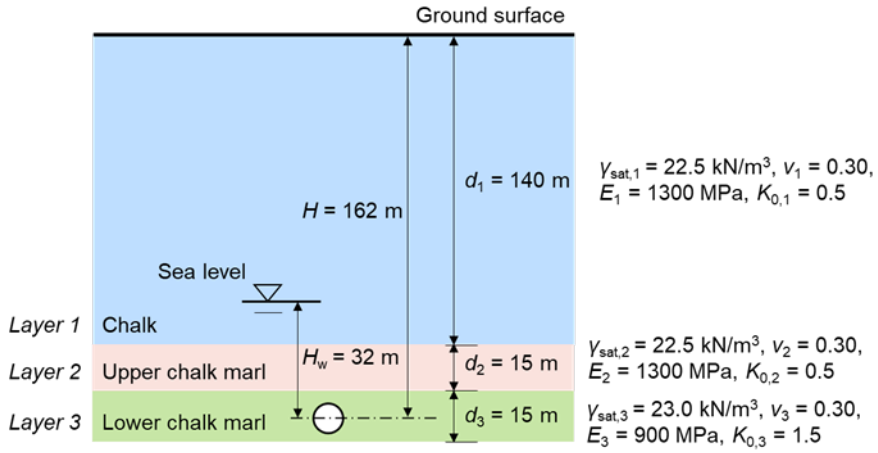

Figure 3.4 Geologic profile for tunnel section 4 (data from (BTS, 2004))

3.2 Model verification and reinforcement design for tunnel sections

This section first compares three different methods for calculating the internal forces across a tunnel section under ambient conditions by using: (1) the Elastic Equation Method, (2) numerical modeling in FLAC3D, and (3) numerical modeling in SAFIR (a program specific for analysis of structures at elevated temperatures). The three methods are used to solve the internal forces of a sample tunnel section under ambient conditions to verify a beam-spring model in SAFIR. The verified SAFIR beam-spring model will later be used to design the reinforcement of tunnel sections 1-4 (given that there is no reinforcement detail available in the literature) and analyze the sections under elevated temperatures.

3.2.1 Verification of the beam-spring model

Case description

The analyzed tunnel section is adapted from a verified model described in the FLAC3D manual (ITASCA, 2017). A circular tunnel is located at 30 m depth in a soft elastic soil. The tunnel lining is constructed with concrete (E = 35 GPa, ν = 0.2), and has a centerline radius of 3.95 m and a thickness of 0.4 m. The surrounding soil has an elastic modulus of 40 MPa and Poisson's ratio

of 0.3. The in-situ stresses are 600 kPa vertical and 300 kPa horizontal. Both the concrete and soil are assumed to be isotropic and linear elastic in this verification study.

Model description

The aforementioned three methods are used to determine the bending moments and axial forces across the tunnel section. The Elastic Equation Method is recommended by JSCE (2007) and ITA (2000) for the design of circular tunnel sections, where the bending moment and axial force across the section are solved using the force method. FLAC3D is an explicit continuum modeling software with a focus on geotechnical analysis. FLAC3D can capture the internal forces of the concrete liner and the stresses within soil zones when the concrete liner is modeled as shell elements and soil as continuum zone elements (ITASCA, 2017). SAFIR is a finite element software developed for structural analysis under elevated temperatures. SAFIR can incorporate characteristics of the RC lining sections within beam elements, but the subgrade reactions can only be represented by a series of one-dimensional elastic elements, such as springs (Hua et al., 2021). The schematics of the FLAC3D and SAFIR models are illustrated in Figure 3.5, and the details for the Elastic Equation Method can be found in JSCE (2007).

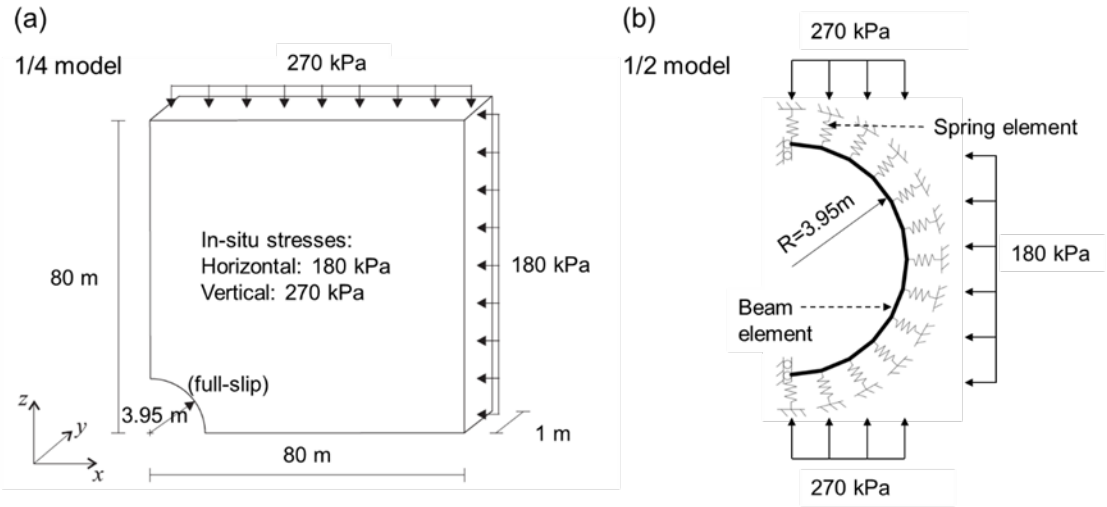

Figure 3.5 (a) FLAC3D model and (b) SAFIR model for the sample tunnel section

The FLAC3D model simulates a thin slice of a circular tunnel in an infinite elastic ground mass with a preexisting anisotropic biaxial stress field subjected to plane-strain conditions. As

Figure 3.5a shows, one quarter of the tunnel lining and the soil body are modeled with symmetric boundary conditions. Plane-strain conditions are enforced by including a thin slice of material in the y-direction and imposing symmetry boundary conditions on these two surfaces. Symmetry boundary conditions are also imposed on the planes at $x = 0$ and $z = 0$. The far-field boundaries are placed at a distance of about 20 times the tunnel radius to approximate infinite boundaries. The in-situ stresses are installed in all soil zones and applied as loads acting on the far-field boundaries. A full slip condition is assumed on the interface between the concrete liner and soil (ITASCA, 2017).

Figure 3.5b shows the SAFIR beam-spring model of half of the investigated tunnel section, where the concrete liner is composed of 12 beam elements and the subgrade reaction is captured by 13 radial spring elements. The stiffness of the springs (K_r) is calculated using Eq. 3.1 (Savov et al., 2005), as a function of tunnel radius R, modulus of elasticity E, and Poisson's ratio ν of the surrounding soil. The springs are only activated when the tunnel expands outward, placing the springs in compression. The horizontal movement and rotation are restrained at the two ends of the liner elements to simulate symmetric boundary condition. The soil pressure is applied as external loadings on the beam elements. A mesh sensitivity analysis was conducted to confirm that the current number of elements is sufficient for convergence.

$$K_r = \frac{E}{[R(1+\nu)]} \tag{3.1}$$

Comparison of results

The bending moment and axial force in the tunnel lining calculated using the three methods are compared in Figure 3.6, where "EEM" in the legends stands for the Elastic Equation Method. The horizontal axis of the figures describes the angle defined from the crown of the tunnel section to the location under consideration (θ in degree). The results are only shown for a quarter of the tunnel section ($\theta \in [0,90°]$), considering the model symmetry. Overall, the three methods predict similar results for both bending moment and axial force. The Elastic Equation Method and SAFIR model generally predict more conservative results than the FLAC3D model.

The beam-spring modeling approach in SAFIR is considered as verified and will be used to design the reinforcement of tunnel sections 1-4 and analyze the sections under fire.

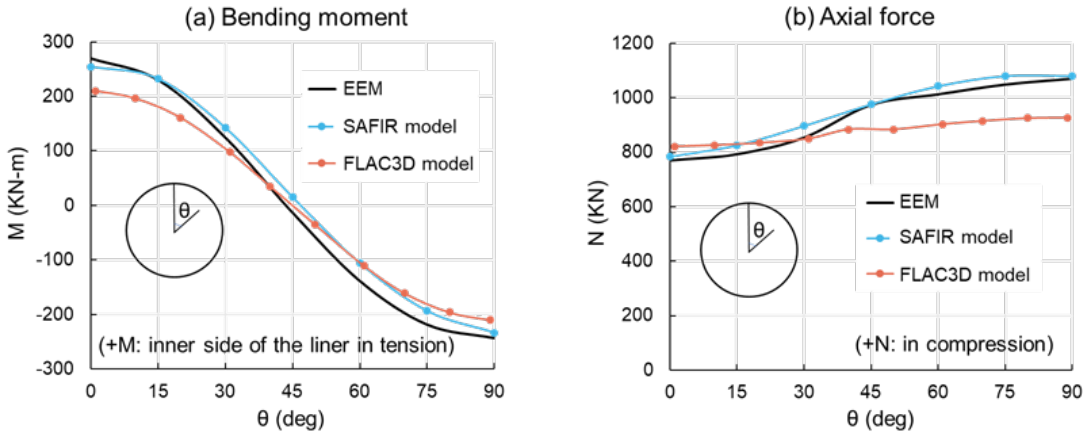

Figure 3.6 Comparison of results between Elastic Equation Method, SAFIR, and FLAC3D based on (a) bending moment and (b) axial force in the tunnel section

3.2.2 Reinforcement design

The SAFIR beam-spring model is used to design the reinforcement of tunnel sections 1-4, given that there is no reinforcement detail available in the literature. The four tunnel lining sections are assumed to have the same inner diameter of 7.5 m and a thickness of 0.35 m for the purpose of this section (note that tunnel sections 1-4 have diameters ranging from 7.3 m to 7.7 m).

The design process is divided into the three following steps:

1. Determine the applied loads and the load combinations for the tunnel sections. In doing so, the unfactored water and earth loads are calculated according to AASHTO (2017) and FHWA (2009). The load distribution is adopted from JSCE (2007) and ITA (2000). The "Strength T-I" from AASHTO (2017) is used for the load combination.
2. Compute the bending moments and axial forces across the tunnel sections using the previously verified SAFIR beam-spring model. The model considers different

subgrade stiffnesses (using Eq. 3.1) and load applications for the four tunnel sections. Concrete has an elastic modulus of 25 GPa and a Poisson's ratio of 0.2.

3. Select the reinforcement across the tunnel sections. The reinforcement ratios are determined using the interaction diagram considering a combined effect of bending moment and axial force (ACI, 2019). The same reinforcement layout is applied to all the segments within each tunnel section.

Following the above steps, the reinforcement for tunnel sections 1-3 is designed as #16@100mm (ϱ = 0.011), and for tunnel section 4 is designed as #25@100mm (ϱ = 0.023).

3.3 Fire performance of the tunnel sections: methodology

This section described the methodology to evaluate and compare the fire performance of the four tunnel sections under different fire scenarios. First, the fire behavior of the four tunnel sections is simulated under the RABT-train fire curve (shown in Figure 3.7). The simulations are continued for 72 hours to capture the full cooling of the RC sections. The results are used to compare the structural performance of tunnel sections during heating, cooling, and after fire. Second, the four tunnel sections are simulated under the RWS fire curve (shown in Figure 3.7) and are continued for 100 hours or until failure to quantify the failure time. Third, a preliminary analysis is completed to investigate the heat induced excess pore pressure and change in subgrade reaction modulus under elevated temperatures, as well as their influence on the structural fire performance of tunnel section 2. This analysis is only conducted on section 2, for which high-temperature soil data is available from material tests.

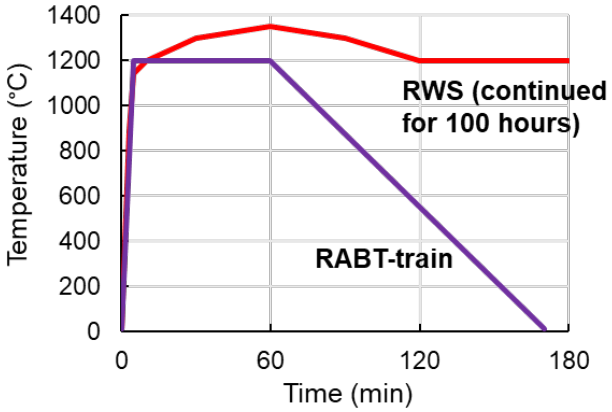

Figure 3.7 The RABT-train and RWS fire temperature-time curves

3.3.1 RABT-train fire curve

This study is conducted using sequentially coupled thermo-structural analyses via SAFIR. In this procedure, a 2D transient thermal analysis is first carried out for the beam cross-section. As a result, the time-dependent temperature of each sectional fiber is obtained and used as an input for the subsequent nonlinear mechanical analysis.

Thermal analysis

The 2D model and its discretization for thermal analysis. Taking tunnel section 1 for example, a 0.35-m thick and 1-m wide RC lining section is modeled with refined mesh at the bottom (the side that is exposed to fire). The rebar sections are modeled with a rectangular mesh to simplify the meshing process. The bottom side of the tunnel lining section is exposed to the RABT-train fire curve and its top is covered with a 0.7-m thick soil layer. The top side of the soil layer is set to be insulated. A preliminary study investigated the influence of soil thickness on the heat transfer results and confirmed that including more than 0.7 m of the soil layer (double the lining thickness) wound only slightly change the temperature distributions across the section (less than 2%).

The thermal elongation, specific heat, and thermal conductivity of concrete and steel are defined as temperature-dependent per EN 1992-1-2 (CEN, 2004) and EN 1993-1-2 (CEN, 2005). The thermal conductivity of concrete is considered as non-reversible during cooling; thus, its

value during cooling remains at the magnitude corresponding to that of the maximum temperature during heating. The thermal properties of soil are not considered as temperature-dependent for two reasons: (1) the relatively low temperatures in soil, and (2) the lack of relevant guideline or test data. The thermal analysis is conducted for 72 hours, until the RC section is completely cooled down to ambient temperatures. This way, the temperature distribution during both heating and cooling can be captured and used as an input for the following mechanical analysis.

Mechanical analysis

The beam-spring model is used to analyze the structural performance of the four tunnel sections under the RABT-train fire curve, as Figure 3.8 shows. The tunnel section is divided into two regions, denoted as "hot" and "cold" in the figure. The hot region adopts the sectional temperatures from the thermal analysis, and the cold region remains at ambient temperature throughout the fire. According to (Hua et al., 2020; 2021), the ceiling of a tunnel would be exposed to the highest temperature whereas its bottom half hardly feels any heat during a fire. Note that the subgrade reaction is captured through the springs.

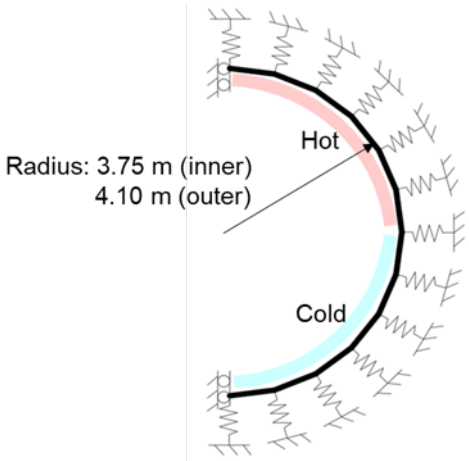

Figure 3.8 The beam-spring model for the mechanical analysis under fire

As for the material properties at ambient temperature, the compressive strength of concrete is taken as 27.5 MPa and the tensile strength is assumed to be zero. The tensile yield strength of the reinforcement is 414 MPa. The stress-strain material relationships for every fiber

in a beam section is generated considering material type (steel or concrete), temperature, and the corresponding mechanical properties. The temperature-dependent material properties from EN 1992-1-2 (CEN, 2004) are taken for both concrete and steel. During cooling, an additional 10% loss in the concrete compressive strength with respect to the value at the maximum temperature is considered, as per EN 1994-1-2 (CEN, 2005). The residual thermal expansion or shrinkage is considered when concrete returns to ambient temperature (Gernay and Franssen, 2016). The Young's modulus and the yield strength of steel are considered fully recoverable during cooling, if the maximum reached temperature is lower than 1200 °C. Soil spring stiffness is calculated using Eq. 3.1 for each investigated tunnel section. The spring properties are independent of soil temperature for this part of the study.

The output of the analysis will compare the time-dependent sectional temperatures and the tunnel deformation during and after the exposure to the RABT-train fire curve for tunnel sections 1-4.

3.3.2 RWS fire curve

In this section, a series of SAFIR thermo-mechanical analyses is carried out using the beam-spring model for the four tunnel sections. The model discretization, material properties, and load applications are kept the same as before. The only difference is that the top half of the tunnel is exposed to the RWS fire curve with a prolonged heating plateau, which lasts for 100 hours in total. The results of this study will focus on a comparison of the failure time of the tunnel sections in various ground conditions.

3.3.3 Effect of temperature on soil properties

Capturing the soil behavior under elevated temperatures often involves complex coupled thermo-hydro-mechanical (THM) processes. Although the effects of temperature on soil properties for use in tunnel lining applications are not well investigated, existing studies have investigated the THM processes within the field of energy geotechnics (McCartney et al., 2019;

Manepally et al., 2011; Joulin, 2019). Useful theories and experimental data can be obtained from such studies for the purpose of this work. However, when it comes to the modeling of tunnel fires, significant complexities exist, and it is impossible to include all the coupling relationships in the THM process using current structural engineering modeling tools. Given these limitations, this section proposes a simplified methodology to include the effect of thermal induced pore pressure and the temperature-dependent soil stiffness in the mechanical analysis. The proposed methodology requires experimental data on temperature-dependent soil properties, which are limited in the literature. Hence, the methodology is only applied to tunnel section 2, where the relevant data for clay is available.

Figure 3.9 shows a flowchart of how the temperature effect on soil behavior (taking saturated clay for example) is considered in this study. When clay temperature increases, excess pore water pressure is generated due to the differential expansion of the pore water and soil solids. This excess pore pressure reduces the effective stress in the soil solids. The reduction of the effective stress could decrease the elastic modulus of the clay, while thermal hardening could increase the elastic modulus. Therefore, the elastic modulus of soil is a function of both soil temperature and excess pore pressure. The net change in clay's elastic modulus would affect tunnel deformation under fire. Note that in this study, the soil behavior does not influence the heat transfer process in reverse, for model feasibility.

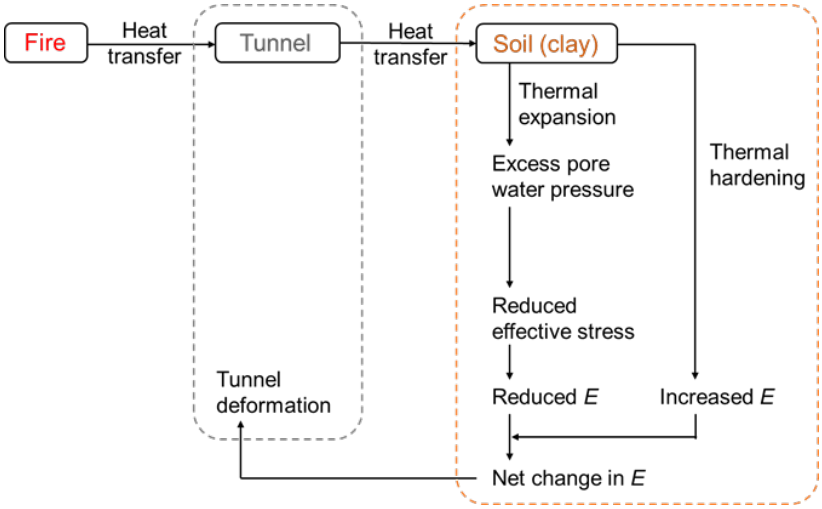

Figure 3.9 Considered changes in soil behavior under elevated temperatures for application in the structural analysis of tunnel sections under fire

The relevant data collected from literature are shown in Figure 3.10. The data in Figure 3.10a was collected by Ghaaowd et al. (2017), including 13 clay specimens (denoted in the figure as "SPC1" through "SPC13"), and 8 types of clay, namely: remolded illite clay, Pacific smectite clay, illite clay, Bourke silt, Bangkok clay, Todi clay, Fiumicino clay, and Newfield clay. The figure shows the effect of temperature (0-80 °C) on the change in pore water pressure. The lower and upper bounds for the slope Δu (kPa)/ΔT (°C) of the data points are indicted by S1 = 0.9 kPa/°C and S2 = 4.3 kPa/°C. The data in Figure 3.10b is obtained from Cekerevac and Laloui (2004), where Kaolin clay samples were tested using a temperature-controlled triaxial apparatus. The secant elastic modulus obtained from tests at 22 °C and 90 °C are presented in the figure, including normally consolidated (NC) and over consolidated (OC) samples. This figure shows the influence of both effective stress and temperature on clay's elastic modulus. For the interest of this study, the results of NC samples are adopted with a linear interpolation of data for the temperatures between 22 °C to 90 °C.

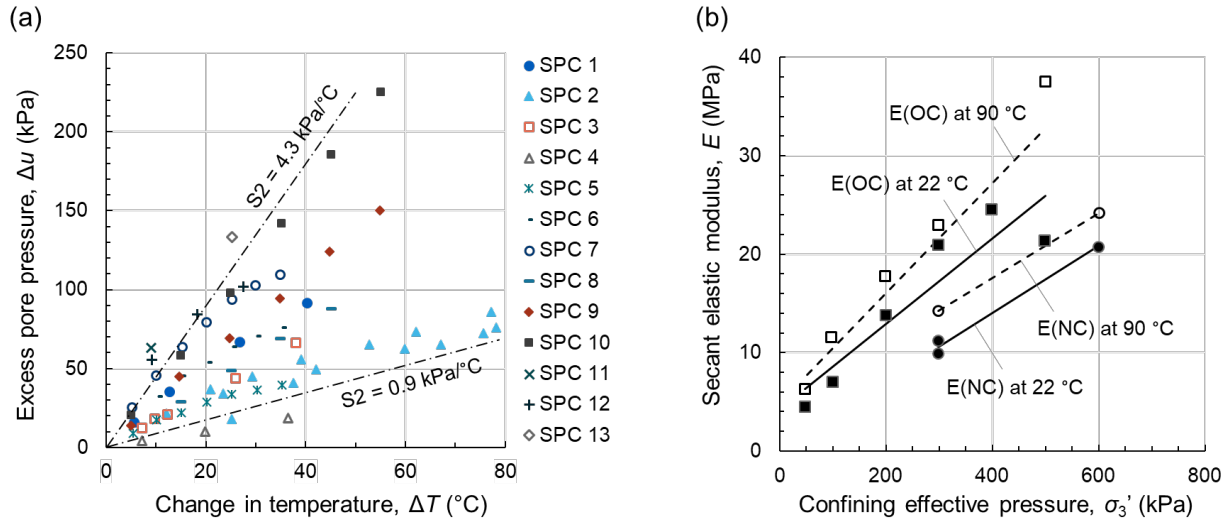

Figure 3.10 Test data on (a) excess pore pressure, data extracted from (Ghaaowd et al., 2017) and (b) secant elastic modulus of clay, data extracted from (Cekerevac and Laloui, 2004)

The methodology of Figure 3.9 is implemented into the numerical model by updating the beam-spring model to a beam-truss model, i.e., replacing the spring elements with elastic truss elements. The truss elements have the same compressive elastic modulus as the springs at the

ambient temperature but are capable of updating a time-dependent elastic modulus (whereas spring elements are not). The tensile elastic modulus of the truss material is assigned a very small value to achieve compression-only behavior.

The updated model of tunnel section 2 is simulated under 11 hours of exposure to the RWS fire curve. This simulation does not last for 100 hours, because the soil temperature reaches 90°C at 11 hours and soil data is not available beyond 90°C. The adopted excess pore pressure-time curves and soil elastic modulus-time curves for the upper and lower bounds are shown in Figure 3.11. It is clear that the thermal hardening dominates the change in the elastic modulus of clay, when considering a low excess pore pressure, while the reduction in effective stress becomes dominant when large excess pore pressure is considered.

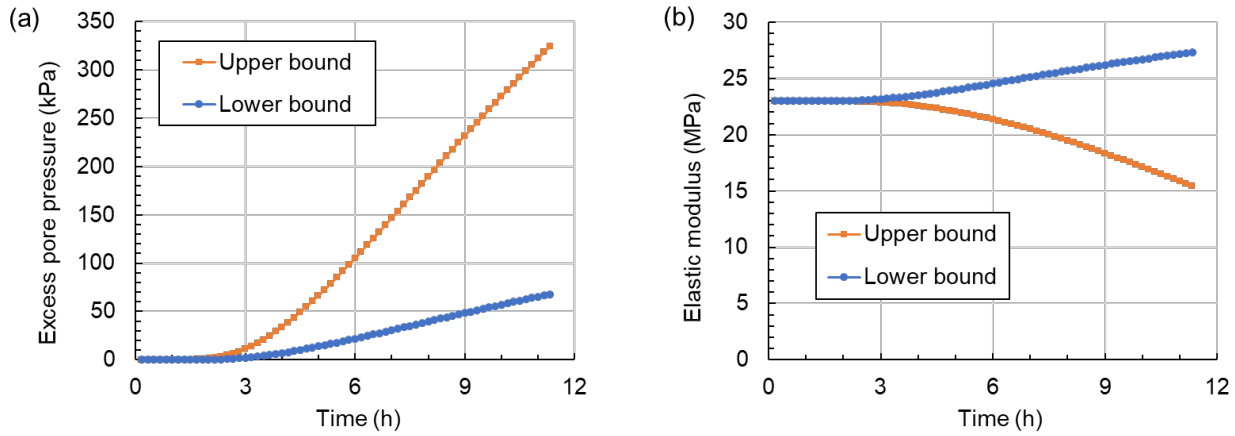

Figure 3.11 Time-dependent (a) excess pore pressure and (b) elastic modulus of clay for tunnel section 2

3.4 Results

3.4.1 RABT-train fire curve

The structural response of tunnels under fire is governed by a combination of several mechanisms. Initially, the load-induced stresses in the intact structure are due to the earth pressure, water pressure, self-weight and applied live loads. When the fire starts and heat propagates through the lining sections, thermally-induced axial forces and bending moments (due to the thermal gradient) are generated. The restraint within a tunnel lining section also changes with time as the temperature increases, and the surrounding structure heats up.

Simultaneously, the non-uniform material degradation close to the fire-exposed surface makes the section weaker and shifts the center of stiffness of the section. The following sections will present the temperature distributions within the heated elements and the structural response for the four tunnel sections.

Temperature distributions in the heated tunnel lining elements

The temperature evolutions of the center concrete, inner, and outer circumferential reinforcement within the heated part of section 1, when subjected to the RABT-train fire curve, are shown in Figure 3.12. The results obtained from the heat transfer analyses of sections 2-4 show that the thermal properties of background soil have a minor influence on the temperatures of concrete and reinforcement. The differences between the sectional temperatures of the four tunnel sections are less than 5%.

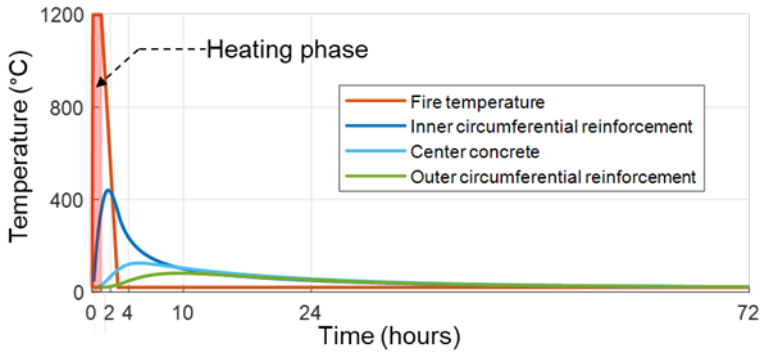

Figure 3.12 Temperature distribution within the heated part of tunnel section 1 under the RABT-train fire curve

Although the heating phase of the RABT-train fire curve only lasts for one hour, the center concrete reaches its peak temperature at about t = 4 hours, when the fire curve has entered its cooling phase for 3 hours. The peak temperature of the inner reinforcement has just exceeded 400 °C at t = 4 hours, given a 50 mm-thick cover, meaning that steel reinforcement maintains its strength during the fire. The delayed heating response is common in concrete structures due to the low thermal conductivity and the greater thickness compared to steel sections. This

phenomenon raises concerns on the structural performance during the cooling phase of fire. In this case, the tunnel section is cooled down to ambient temperature after 72 hours.

Structural response

Overall, the four tunnel sections do not fail under the RABT-train fire curve. Table 3.2 summarizes the obtained results to provide a comparison between the behavior of the four tunnel sections under the RABT-train fire curve. The table compares internal forces, deformations, rebar temperatures, stresses, and the damaged depths analyzed at the crown elements. The fire damaged depth is evaluated using two different methods: (1) temperature based, by setting up a threshold of 300 °C, as introduced in (Hua et al., 2021); (2) stress based, using the bell-shaped stress profiles. The table also includes the difference (Δ) between results at "ambient" temperature and "heated" cases.

Table 3.2 Summary of the results for the four tunnel sections under the RABT-train fire curve

	Section 1: Shallow tunnel, soft soil			Section 2: Moderate-depth tunnel, soft soil		
	Ambient	Heated	Δ	Ambient	Heated	Δ
Moment (kN-m)	110	250	140	220	420	200
Axial force (kN)	1110	1160	50	2270	2310	40
Ovality (%)	0.130	0.230	0.100	0.500	0.750	0.250
Rebar temperature (°C)	20	450	/	20	450	/
Rebar stress (MPa)	70	300	230	140	414	274
Fire damaged depth (T based) (mm)	0	75	/	0	75	/
Fire damaged depth (σ based) (mm)	0	50	/	0	50	/

(Continued)

	Section 3: Moderate-depth tunnel, rock			**Section 4: Deep tunnel, rock**		
	Ambient	Heated	**Δ**	Ambient	Heated	**Δ**
Moment (kN-m)	130	350	**220**	280	**500**	**220**
Axial force (kN)	2430	4620	**2190**	6220	**6470**	250
Ovality (%)	0.160	0.162	0.002	0.200	0.290	0.090
Rebar temperature (°C)	20	450	/	20	450	/
Rebar stress (MPa)	200	380	180	200	**414**	214
Fire damaged depth (T based) (mm)	0	75	/	0	75	/
Fire damaged depth (σ based) (mm)	0	**130**	/	0	**130**	/

The following conclusions are made based on the results:

- None of the tunnel sections failed after being exposed to the RABT-train fire curve. However, irrecoverable damage occurred within the lining sections, required repair after the fire.
- Tunnel sections 1 and 2 in soft ground are free to expand during the fire (when compared with sections 3 and 4), leading to larger deformations than those of sections 3 and 4.
- Comparing tunnel sections 1 and 2, section 1 is considered safer because of a relatively low level of applied load. Section 2 has the largest deformation, with the reinforcement yielding at the crown section.

- Tunnel sections 2 and 3 have similar levels of applied load. Section 3 experiences much less deformation but a significant increase in the axial forces due to the more rigid constraint within rock.
- Tunnel section 4 is the only one that is subjected to large lateral pressures (K_0 = 1.5), and it therefore has a different deformed shape than the others. Although the section experiences a high level of compression with the rebars yielding, it re-distributes the internal forces and maintains stability.

Overall, tunnel sections 2 and 4 are deemed as more critical in terms of developing large deformation and internal forces, respectively.

3.4.2 RWS fire curve

Figure 3.13 shows the temperature evolutions within the heated portion of tunnel section 1 under the extended RWS fire curve for 100 hours. Similar to earlier findings, the temperature results from different tunnel sections do not vary significantly (differences within 10%). The temperature of the inner circumferential reinforcement reaches about 900 °C at t = 10 hours, implying that less than 6% of its original strength remains to resist load after 10 hours (CEN, 2005). The center concrete is heated to 300 °C at t = 10 hours, meaning that half of the cross section is damaged and requires repair. The cross-section experiences more material degradation and decrease in stiffness as the fire continues.

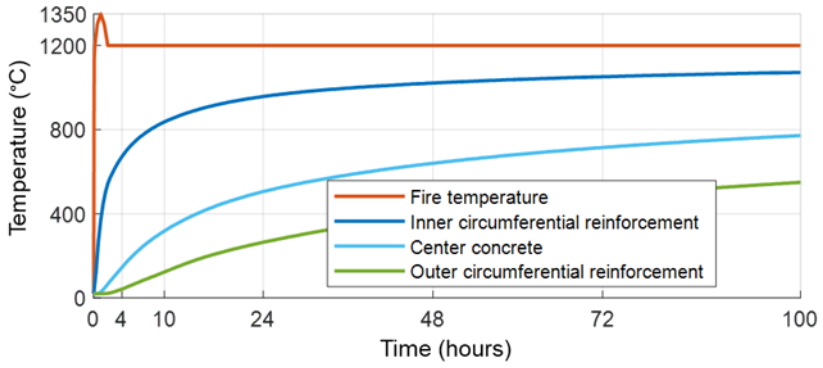

Figure 3.13 Temperature evolution within the heated part of tunnel section 1 under the RWS fire curve

Table 3.3 summarizes the failure times, the critical elements, and the maximum ovalities of the four tunnel sections. Note that sections 1 and 3 do not fail even after 100-hour heating of the RWS curve. The critical element is defined as the element that firstly fails and triggers the collapse of the whole structure.

Table 3.3 Summary of the tunnel fire performances under a 100-hour RWS fire

	Section 1: Shallow tunnel, soft soil	Section 2: Moderate-depth tunnel, soft soil	Section 3: Moderate-depth tunnel, rock	Section 4: Deep tunnel, rock
Failure time	Does not fail	45 hours	Does not fail	52 hours
Critical element	Does not fail	Crown	Does not fail	Spring-line
Max. ovality (%)	0.22	1.50	0.17	0.60

Overall, the four tunnel sections show good fire resistance with 45 hours as the earliest failure time. Tunnel section 2 fails at the crown element, whereas section 4 fails at the spring-line element. The two failures occur soon after the compressive (outer circumferential) reinforcements yield. The time to failure also reveals information on the time span during which it would be safe for the fire-fighters to enter the site. However, the calculations in this section assume a constant subgrade stiffness and soil/water pressure, which could make the critical life-safety time unconservative. The following section investigates the effect of temperature-dependent soil behavior on the response of the tunnel section 2.

3.4.3 Effect of temperature on soil properties

This section shows the results from the implemented methodology described in Section 3.3.3. Figure 3.14 compares the vertical crown displacements of tunnel section 2 calculated using the lower bound, upper bound, and the original solutions, where the lower and upper bounds

correspond to the levels of considered excess pore pressures, and the original solution considers constant subgrade stiffness and soil/water pressure.

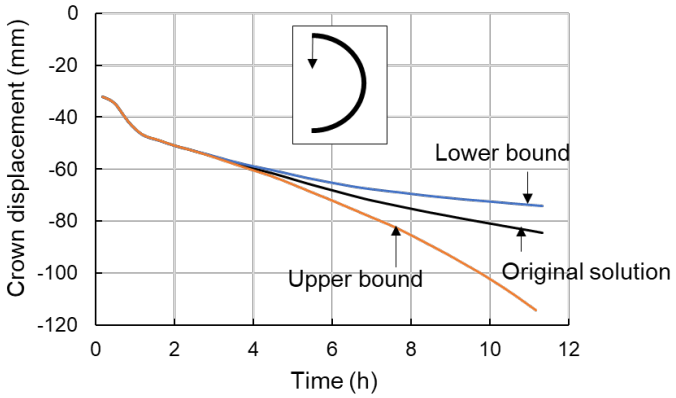

Figure 3.14 Comparison of vertical crown displacement for tunnel section 2 considering constant soil properties (original solution) and temperature-dependent soil properties (lower and upper bounds)

Although none of the cases reached the limit state within 11 hours, by considering the upper bound of temperature effect on soil behaviors, the crown displacement increased from 85 to 115 mm at 11 hours. The crown also experiences an increasing displacement rate starting at about t = 4 hours. The result for the lower bound of the excess pore pressure follows a similar displacement profile of the original solution during the considered time span. Note that the lower bound is likely unrealistic as thermally hardening a small zone of soil surrounding the tunnel will have little influence, because the adjacent soil at normal temperatures is unaffected. These results emphasize the need for considering temperature-dependent soil behaviors when analyzing tunnel fire performance.

3.5 Conclusion

This chapter compared the fire performance of bored tunnel lining sections under four ground conditions, ranging from shallow soft soil to deep rock. The fire performance was analyzed using a verified beam-spring model implemented in the finite element program SAFIR.

The investigated tunnel lining sections were adopted from realistic high-profile tunnels. A series of analyses were conducted to evaluate the performance of tunnel sections under a wide range of fire scenarios and ground conditions. The considered ground conditions included: (1) shallow tunnel in soft soil, (2) moderate depth tunnel in soft soil, (3) moderate depth tunnel in rock, and (4) deep tunnel in rock. The considered fire scenarios included: (1) the RABT-train fire curve and (2) an extended RWS fire curve. Heat transfer analyses were performed until the tunnel sections were completely cooled down. The chapter also proposed a simplified methodology to include temperature-dependent soil properties. Relevant data on clay soil was collected to study the effects of heat induced excess pore pressure and the change in subgrade reaction modulus on the structural fire performance of the moderate depth tunnel section in soft soil. The following conclusions can be drawn based on the results of this study:

- RC tunnel linings experience delayed structural response due to the slow heat conduction in concrete sections. The investigated tunnel lining sections continued to deform after entering the cooling phase, raising a concern for the safety of fire-fighters.
- RC tunnel linings experienced significant fire damage following the considered fire scenarios, requiring careful assessment and repair work. The fire-induced deformations were not fully reversable due to permanent fire damage to both concrete and reinforcement. The moderate-depth lining section in soft ground underwent the largest deformations, and the moderate-depth lining section in rock had the smallest deformations during and after exposure to the RABT-train fire curve.
- The tunnel lining sections in soft ground were partially in tension during the fire, while the tunnel sections in rock were in compression, which made cases in hard rock have better performance during the considered fire events, when compared with those in soft soil.

CHAPTER 4 DAMAGE ASSESSMENT

4.1 Introduction

The goal of post-fire assessment is to identify whether a structure should be repaired or demolished. When repair is a viable option, the level of damage determines the most efficient repair strategy. The outcome of an assessment should include an estimate of the extent and degree of damage, such as the spalled/deteriorated depth of a cross-section, the maximum temperature reached in fire-affected areas, and the residual strength of concrete. Identifying proper damage levels and corresponding repair classifications are needed to set up performance objectives for design and assessment of tunnels under fire. Although no detailed damage assessment framework is available for tunnel structures, a few official documents exist for fire damage assessment and repair guidelines for general concrete structures (NCMA, 1994; Concrete Society, 2008; fib, 2008; ACI, 2013; ACI, 2016).

This chapter discusses a fire damage assessment framework for reinforced concrete (RC) tunnel linings, which integrates advanced modeling with visual inspections, non-destructive testing, and material sampling. The framework quantifies fire damage to RC tunnel linings in terms of surface discoloration, crack width, concrete spalling, sectional temperatures, strength loss of materials, and residual displacement. A damage classification system is discussed based on a collection of international guidelines and feedback from industry experts to facilitate a systematic determination of the necessary damage metrics and repair strategies. A case study, using data from recent experiments, is conducted to demonstrate the applicability of the proposed framework and the benefits of the information obtained from numerical modeling. This framework can be integrated with risk-assessment methods to optimize the fire design of tunnels with associated active and/or passive fire protection.

4.2 Framework

Figure 4.1 summarizes the proposed damage assessment framework for RC tunnel linings exposed to fire. It is suggested that practitioners utilize advanced modelling in three steps and

combine the results with traditional post-fire damage assessment procedures to evaluate safety and obtain a full understanding of fire damage to a tunnel lining. The overall damage conditions obtained from the two paths in Figure 4.1 can be incorporated into a damage classification system to assist in determining the level of required repair work. The following paragraphs will discuss each step in more detail.

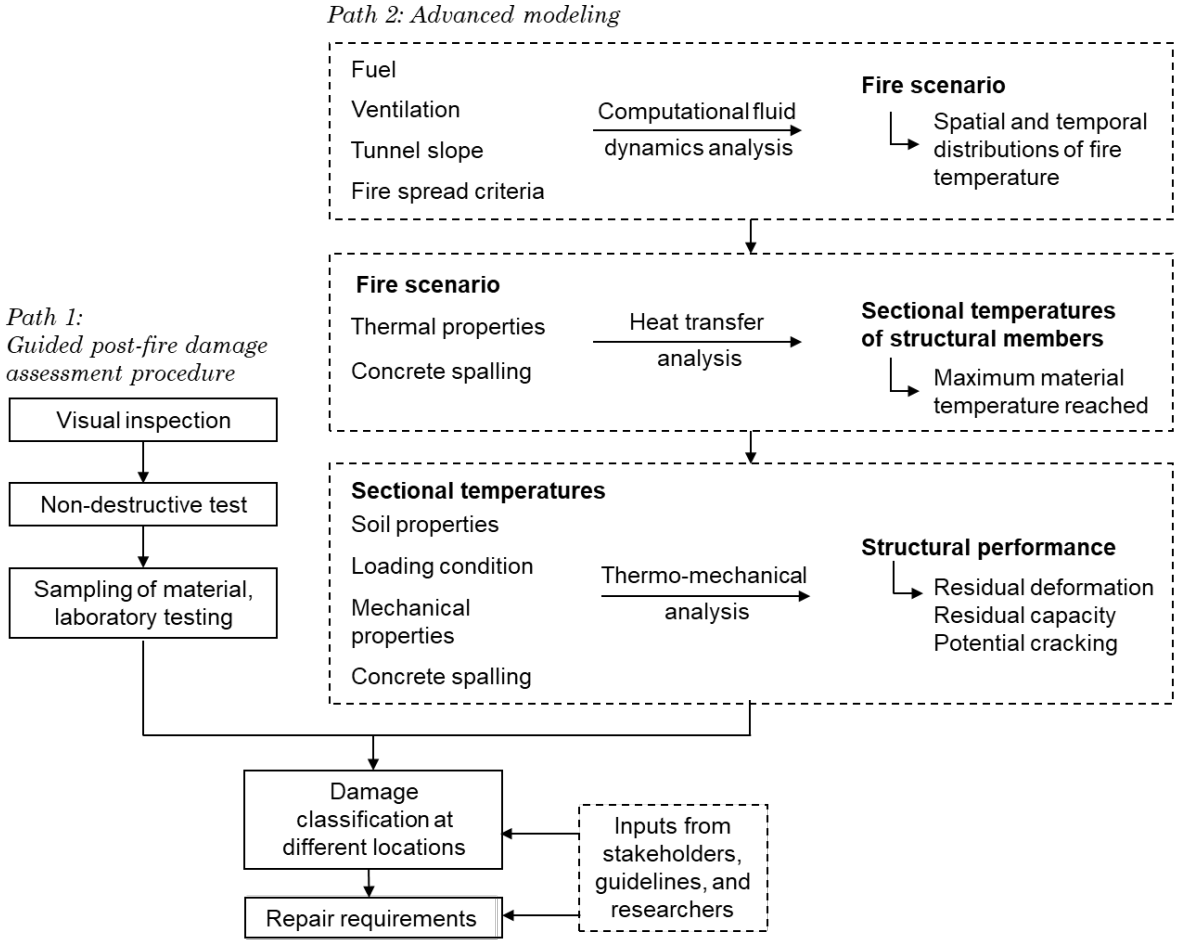

Figure 4.1 Damage assessment framework for RC tunnel linings exposed to fire

4.2.2 Guided post-fire damage assessment procedure

There are several guidelines and official documents available for fire damage assessment of concrete structures, with application examples for RC building elements. These guidelines use similar approaches: visual inspection, non-destructive testing, and laboratory testing of material samples.

Visual inspection: Visual inspection provides recordings of features such as concrete color, concrete spalling, cracking, surface crazing, distortion, deflections, and collapse. The surface appearance of concrete provides engineers with the first indication of which elements require cosmetic repair, and which, if any, will need further assessment. The color of concrete can change as a result of heating, which is apparent upon visual inspection. Concrete shows pink/red discoloration due to oxidation of ferric salts in aggregates above 300 °C, also indicating a strength loss of the material (Concrete Society, 2008; fib, 2008). Heat-induced spalling is a major and common issue for the fire performance of concrete structures (Bisby et al., 2014). Spalling conditions range from localized ejection of small and thin chips to dramatic discharge of large pieces of concrete and exposing reinforcement. Spalling also enables the fire frontier to propagate deeper into the concrete and thus increases the deteriorated depth. Visual inspection after fire should include an assessment of spalling, documented as the spalling depth across the affected area, as well as the total weight/volume of spalled concrete.

Non-destructive testing (NDT): Numerous NDT techniques are used to provide additional damage evaluations on the findings of visual inspection. Details of implementation and reliability of applicable NDT methods can be found in the ACI 228.2R (ACI, 2013). Due to the common availability and the ease of application, the most commonly used NDT methods for fire damage assessment are the rebound (Schmidt hammer) test and the ultrasonic pulse velocity (UPV) test (Concrete Society, 2008; fib, 2008; Albrektsson et al., 2011). These methods can provide an estimation of concrete strength loss in situ but are largely influenced by other factors such as surface smoothness, size, and shape of test specimens, and therefore their results are not always consistent. NDT is a fast-growing field as a result of technological developments including digital image processing and machine learning algorithms (Felicetti, 2013; Hoang et al., 2019).

Sampling of material and subsequent laboratory testing: Samples of damaged material, together with undamaged references, may be removed for laboratory investigation to provide a more reliable evaluation. Concrete samples are typically obtained by drilling of cores or by careful extraction of lump samples (Ingham, 2009). Concrete core samples can be taken for petrographic examination and compression tests. The petrographic analysis is mainly concerned with the

damage and property change of concrete at high temperatures, i.e., depth of microcracking, paste alteration (color change and strength softening), and carbonation (ASTM, 2020).

4.2.3 Advanced modelling

The extent of fire damage to a RC tunnel lining structure (e.g., residual deformation of the crown element) is influenced by a series of parameters that include the fire temperature and duration, material properties (e.g., normal strength concrete vs. high strength concrete), shape of the tunnel cross-section (e.g., rectangular vs. circular), as well as the surrounding geologic conditions (e.g., soft soil vs. rock) (Caner and Böncü, 2009). As an alternative, or in addition to inspection and testing methods, advanced modeling can provide more detailed assessment for fire damage diagnoses. Numerical modeling can also incorporate comprehensive parametric studies more economically when compared to laboratory testing, which enables damage-based performance design for fire. A three-step approach is proposed to utilize numerical modeling for assessing material damage and the residual status of tunnel linings after fire.

Step 1 - tunnel fire scenarios: A fire scenario describes the evolution of gas temperature over time during a fire event. A tunnel fire scenario is typically characterized by a fast heating rate and a high peak temperature. Due to the special geometry of the tunnel space, gas temperature varies significantly along the tunnel length and across its cross-sections during a fire event. Understanding the temporal as well as spatial distributions of temperature inside a tunnel is important for fire damage assessment. Computational fluid dynamics (CFD) modelling tools, such as FDS and Ansys Fluent, can capture complex 3D fire scenarios (Ministry of Transportation and Public Works of the Netherlands, 1999). After a site survey to evaluate the fire cause, fire center location, combustion load, and the natural or active ventilation conditions during the fire event, CFD modelling can be used to replicate the fire scenario and estimate the fire severity, e.g., the maximum gas temperatures at different locations within the tunnel space.

Step 2 - sectional temperatures of the lining: Once a credible demand fire scenario is determined, temperatures within the sections can be obtained by completing a heat-transfer analysis. The analysis can be conducted using finite element software such as ABAQUS, ANSYS,

and SAFIR (Franssen and Gernay, 2017), the results of which can be conveniently imported into a mechanical analysis in the next step or used for hand calculations. The greatest challenge in this step is to model concrete spalling and incorporate the process into a heat transfer analysis. Considering that concrete spalling is hardly predictable and involves large uncertainties, Hua et al. (2021) developed a data-driven method to evaluate and incorporate an "average" spalling depth within a heat-transfer analysis. Following an actual event, engineers/inspectors can measure the spalled depth of concrete and use a spalling-incorporated heat-transfer analysis to obtain realistic sectional temperatures. The results can be used to evaluate the residual material strength across the lining depth.

Step 3 – structural performance: Coupled thermal-mechanical analyses performed with finite-element software packages such as Abaqus and SAFIR, can help determine the residual deformation and capacity of a damaged structure. This type of advanced modeling takes time-dependent sectional temperatures of structural elements as inputs and involves complexities such as large thermal gradients across sections, distinct material properties during heating and cooling, residual strain and deformations, etc. Due to such complexities, most of existing modeling efforts focus on heating behaviors whereas very limited research has considered a structure's cooling behavior and post-fire condition despite their importance in fire damage assessment (Kodur and Agrawal, 2016). Another challenge is to model the soil-structure interaction under elevated temperatures, where supporting test data and relevant model verification is very limited.

4.2.4 Damage classification and repair requirement

Once the structural performance is evaluated using advanced modeling, the next step is to apply relevant thresholds and determine repair strategies. Coded damage classification criteria in national and international standards have two major benefits: (1) for in situ repair, the degree of damage and levels of repair to various elements/locations of the structure can be effectively evaluated, and (2) for performance-based fire design of tunnel structures, a basis is provided for quantification of performance objectives, which can be correlated to tunnel resilience against fire.

Fire damage classifications for general concrete are proposed in official documents previously mentioned (Concrete Society, 2008; fib, 2008). Tables 4.1 and 4.2 list four damage and repair classes adopted from the Concrete Society (2008), which provides guidance for evaluating fire damage and determining repair strategies.

Table 4.1 Fire damage classification adopted from the Concrete Society (2008)

Damage class	Color	Crazing	Spalling	Exposure and condition of main reinforcement	Cracks
1	Normal	Slight	Minor	None exposed	None
2	Pink/ red	Moderate	Localized to patches	Up to 10% exposed, all adhering	None
3	Pink/ red	Extensive	Considerable	Up to 20% exposed, generally adhering	Small
4	Whitish grey	Surface lost	Almost all surface spalled	Over 20% exposed, much separated from concrete	Severe

Table 4.2 Repair classification adopted from the Concrete Society (2008)

Damage class	Repair classification	Repair requirements
1	Superficial	Superficial repair of slight damage
2	General repair	Non-structural or minor structural repair restoring cover to reinforcement where this has been partly lost
3	Principal repair	Strengthening repair reinforced in accordance with the load-carrying requirement of the member. Concrete and reinforcement strength may be significantly reduced requiring check by design procedure.
4	Major repair	Major strengthening repair with original concrete and reinforcement written down to zero strength, or demolition and recasting

Other available fire damage classifications are similar to the one proposed by Concrete Society and are mostly based on observations. However, using concrete color as an indicator is a fairly crude assessment, especially when the lining surface is partially or fully covered by soot. In addition, most of the criteria are qualitative, and the evaluation would largely rely on the inspector/engineer's experience and judgement. To improve the efficiency of post-fire damage

assessment procedure, especially for moderate and severe cases, more quantitative thresholds should be introduced to facilitate a systematic evaluation rather than an ad hoc process.

Table 4.3 proposes damage classification thresholds associated with sectional temperatures and crown residual displacement, which can be documented using laser scanning technology. Note that some of the proposed thresholds, such as crown residual displacements, require further research and refinement. Tunnel segments diagnosed as Class D damage, where there are severe section loss and residual deformation, would require a complete structural analysis (*Step 3* in the advanced modeling) to evaluate the residual structural capacity and locked-in stresses within the sections. The corresponding repair requirements for the defined damage classes are listed in Table 4.4. To implement the proposed framework, the affected tunnel lining sections shall be divided into a series of segments with a diagnosed damage class for each segment. The repair cost can then be estimated for each segment as well as the entire affected lining.

Table 4.3 Proposed fire damage classification as related to the results of advanced modeling

Damage class	Depth of concrete reaching temperatures > 300 °C	Temperature of reinforcement	Crown residual displacement
A	$d <$ half cover depth	$T < 100$ °C	Negligible
B	half cover depth $\leq d <$ cover depth	100 °C $\leq T <$ 300 °C	$\Delta < 1/4"$
C	cover depth $\leq d <$ half section depth	300 °C $\leq T <$ 600 °C or partially exposed	$1/4" \leq \Delta < 1/2"$
D	$d \geq$ half section depth	$T \geq$ 600 °C or majorly exposed	$\Delta \geq 1/2"$

Figure 4.2 Proposed repair requirement for damage classes

Damage class	Repair requirements
A	Superficial repair, such as surface cleaning and crack sealing
B	Concrete restoring
C	Concrete restoring and rebar replacement
D	Conduct advanced thermal-structural analysis to determine residual strains/stresses and capacity of the lining for decision on repair vs. replacement

4.3 Case study

Results from recently conducted large-scale fire tests of RC tunnel slabs are adopted in this section to apply the proposed framework and illustrate the benefit of utilizing advanced modeling in fire damage assessment.

4.3.1 Test parameters

The test specimens included four 2,440 mm x 1,830 mm x 300 mm flat RC slabs, namely, S1-S4. Specimens S1 through S3 were cast with a concrete mix including 0.22% (by volume) polypropylene (PP) fibers to prevent spalling. Specimen S4 was constructed using conventional concrete (same concrete mix as for S1 to S3 but without PP fibers). Two levels of axial restraint were considered in the tests by using three (for S2) or six (for S1, S3, and S4) centric post-tensioned strands. The initial total forces in the strands for each slab were measured as: 683 kN (S1), 687 kN (S2), 322 kN (S3), and 694 kN (S4). The two levels of post-tensioning represent the difference in axial restraint between horseshoe and rectangular tunnel sections. All the slab specimens had the same reinforcement layout with variation in post-tensioning and the concrete mix as discussed above. The longitudinal reinforcement ratio of the specimens was 1.0%.

The ambient concrete strengths were 66 MPa (9.6 ksi) and 73 MPa (10.6 ksi) for specimens S1-S3, and S4, respectively. The moisture contents measured for the concrete used in specimens S1-S3, and S4, were 2.5% and 1.9%, respectively. The yield strength of the reinforcing steel was 414 MPa (60 ksi). The post-tensioning strands were cold-drawn, low-relaxation 7-wire strands with an ultimate stress of 1,861 MPa (270 ksi).

The test program included two main stages: (1) static loading, and (2) fire testing. To begin, a total vertical load of 310 kN was applied to the specimens via a hydraulic actuator and distributed by two steel rollers spaced at 600 mm. This load was kept in place for 4-6 hours after the fire tests (i.e., during the cooling phase). The heating test began when the static loading phase had reached equilibrium. As Figure 4.3 shows, a square area of 1530 mm x 1530 mm of the bottom surface of the specimen was exposed to heat (marked with "directly heated area" in the figure), while the rest of the bottom surface was insulated during tests (marked with "insulated area"). The slabs were simply supported by two steel frames during the tests.

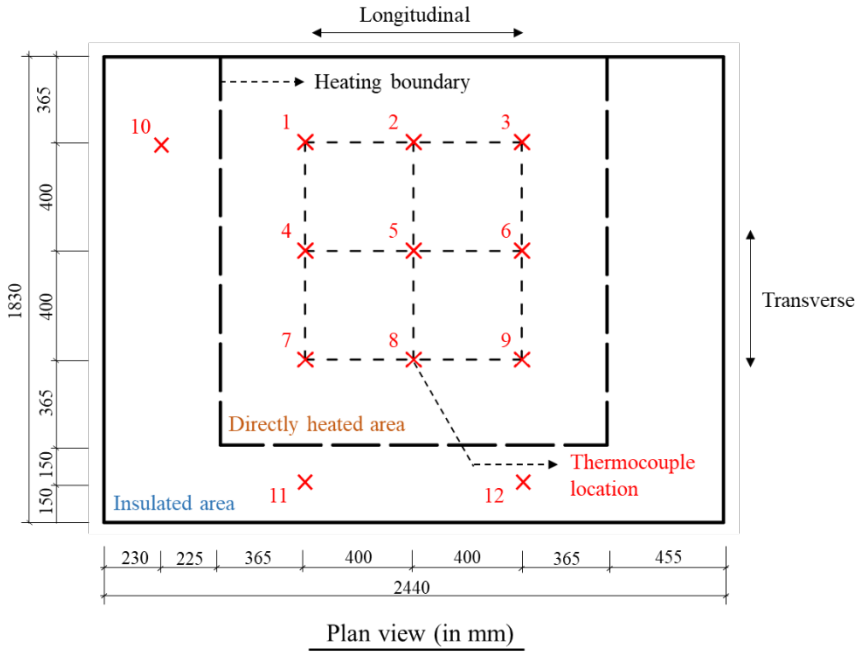

Figure 4.3 Heated area and thermocouple locations in the test slabs

Three moderate fire curves, representing a railway tunnel fire, were applied: "scenario 1" had a heating rate of 40 °C/min and a maximum temperature of 850 °C with a 60-min soak; "scenario 2" had the same heating rate, and a lower peak temperature (700 °C) without soaking; "scenario 3" had the same maximum temperature and soaking duration as scenario 1, but a slower heating ramp. Specimens S1, S2, and S4 were exposed to "scenario 1". As Figure 4.4 shows, specimen S3 was first exposed to "scenario 2" (Test 3A), and then tested with "scenario 3" after

48 hours (Test 3A), where scenario 2 represents activation of a fixed firefighting system in the tunnel and scenario 3 simulates a traveling fire inside the tunnel.

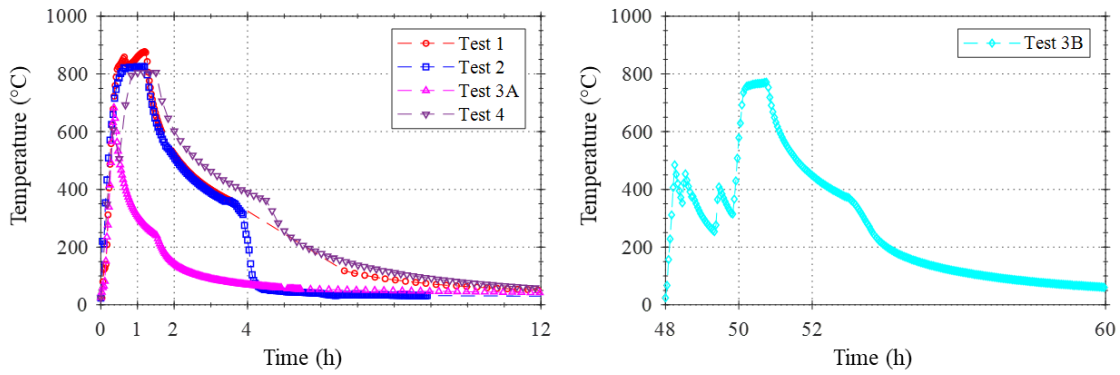

Figure 4.4 Temperature-time protocol for the fire tests

In summary, the test parameters are presented in Table 4.4. Further details on the experiments can be found in Hua et al. (2022b).

Table 4.4 Parameters of the fire tests

Test No.	Specimen No.	Mixed with PP fiber or not	No. of post-tensioned strands	Measured concrete strength (f'_c)	Measured moisture content	Heating curve
Test 1	S1	Yes	6	66 MPa	2.5%	Scenario 1
Test 2	S2	Yes	3	66 MPa	2.5%	Scenario 1
Test 3A	S3	Yes	6	66 MPa	2.5%	Scenario 2
Test 3B	S3	Yes	6	66 MPa	2.5%	Scenario 3
Test 4	S4	No	6	73 MPa	1.9%	Scenario 1

4.3.2 Numerical modelling

The finite element software SAFIR was used to model the thermal-structural response of the test specimens and mimic the damage assessment process. With known temperature boundaries from the test measurements, this section only includes the simulations of *Step 2* and

3 in the proposed damage assessment framework. Further details on the CFD modelling in *Step 1* are provided in Hua et al. (2020).

Step 2 – heat-transfer analysis for sectional temperatures: The heat transfer process was completed using shell elements, implying a one-dimensional heat-transfer analysis across the slab thickness. The temperature-time curves measured during the tests were used as inputs to the model. The boundary temperature of the RC slabs at the surface was calculated through convection and radiation heat transfer modes. The temperature distribution within the slab was then obtained by heat conduction analysis at each time step.

Step 3 – Structural analysis for residual performance: The structural model was divided into multiple areas, representing slab parts exposed to different fire boundaries. Biaxial material models for concrete and reinforcement steel are implemented in the shell finite element. The Explicit Transient Creep (ETC) constitutive model for concrete at elevated temperatures, developed by Gernay and Franssen (2012), was adopted in the analysis. The reduction factors for compressive strength and tensile strength under elevated temperatures are taken from EN1992-1-2 (CEN, 2004). During cooling, an additional 10% loss in the concrete compressive strength with respect to the value at the maximum temperature is considered, as per EN 1994-1-2. Residual thermal expansion or shrinkage is considered when concrete returns to ambient temperatures. The uniaxial steel models for rebar and post-tensioned strands are those described in EN 1992-1-2. The Young's modulus and the yield strength of steel are considered fully recoverable during cooling, if the maximum temperature is lower than 1200 °C. Steel is assumed to lose all its strength, which is not recoverable, after reaching 1200 °C. The applied load and boundary constraints were defined as time-dependent to ensure realistic application. The slab behaviors were modeled up to 24 hours to capture their full response including heating, cooling and residual phases. Further details on the numerical modeling of the experiments can be found in Hua et al. (2022a).

4.3.3 Damage assessment

Table 4.5 summarizes the observations on concrete color change, cracking and spalling, rebar condition, measured residual displacement, and change in concrete strength using the Schmidt hammer test. The observations and measurements are supplemented with the results of numerical modeling to obtain depth of concrete exceeding 300 °C, maximum rebar temperature, and calculated residual displacement. The damage classes are indicated based on those defined in Table 4.3. Test 3A that experienced a quick fire has minimal damage and categorized as Class A damage, requiring surface cleaning and crack sealing. Test 4 that included high strength concrete without PP fibers experienced the most damage, but the structural integrity was not compromised given the small deflection and depth of heat penetration. Thus, Test 4 is categorized as Class C, requiring concrete restoration and rebar replacement.

Table 4.5 Summary of damage assessment using a combination of observations and modeling and recommended repair strategies

Test	Observation			Measurement	NDT
	Color	Cracking/ spalling	Rebar condition	Residual centerline displacement	Concrete strength (average)
Test 1	Pink	0.50 mm	Unexposed	7 mm	-22%
Test 2	Pink	0.55 mm	Unexposed	5 mm	-20%
Test 3A	Grey	0.30 mm	Unexposed	3 mm	+6%
Test 3B	Pink	0.55 mm	Unexposed	5 mm	-15%
Test 4	Pink	Spalling (average depth: 25 mm)	Partially exposed	4 mm	-24%

Test	Advanced modeling			Damage class
	Depth of concrete reaching temperatures > 300 °C	Max. bottom rebar temperature	Residual centerline displacement	
Test 1	25 mm	280 °C	6 mm	B
Test 2	25 mm	275 °C	7 mm	B
Test 3A	0	120 °C	2 mm	A
Test 3B	25 mm	220 °C	6 mm	B
Test 4	50 mm	Partially exposed	6 mm	C

4.4 Conclusion

This chapter introduced a framework for fire damage assessment of reinforced concrete tunnel liners. The framework relies on both observation and measurements as well as numerical modeling of structural response. Damage classes and the corresponding repair methods are indicated based on the depth of concrete exceeding 300 °C, the maximum rebar temperature, and calculated residual displacement. Application of the framework is demonstrated on a set of recently conducted fire experiments. Further research is needed to refine the proposed damage thresholds, especially those related to residual displacement.

CHAPTER 5 CONCLUSIONS AND RECOMMENDATIONS

The research presented in this report provides a framework to evaluate fire damage to reinforced concrete (RC) tunnel liners. The outcomes can be used to assess damage after a fire event or design the structure and fire protection to minimize losses in the case of an extreme fire.

Chapter 2 collected and analyzed existing data on the residual compressive strength of normal strength concrete in the literature. The dataset was analyzed to propose probabilistic models for the residual compressive strength of concrete with siliceous and calcareous aggregates. The models followed the Weibull distribution and were continuous functions that can be implemented in analytical and computational frameworks.

Chapter 3 conducted and compared a series of thermo-mechanical analyses of circular reinforced concrete tunnel lining sections under four geologic conditions, ranging from shallow soft soil to deep rock. A simplified methodology was developed to investigate the heat-induced excess pore pressure and change of subgrade reaction modulus under elevated temperatures, and their influence on the structural fire performance of a tunnel. The TBM reinforced concrete linings exhibit good fire resistance, whereas irrecoverable damage can be expected after exposure to a major fire. The moderate-depth tunnel section in soft soil and the deep tunnel section in hard rock under significant lateral soil pressures were identified as the critical cases due to large deformations and high internal forces, respectively. Ignoring temperature-dependent soil properties in tunnel fire analyses may lead to unconservative results on fire resistance time and deformations of the tunnel section.

Chapter 4 introduced a framework to quantify fire damage to reinforced concrete tunnel linings using surface discoloration, crack width, concrete spalling, sectional temperatures, strength loss of materials, and residual displacement. A damage classification system was proposed to systematically map damage metrics to repair strategies.

Additional research is needed to standardize damage thresholds and the corresponding repair strategies when evaluating structural damage after fire. For example, limits on crack width

and residual deflections and the potential repair costs and times should be further studied and refined. Once repair times and costs are established, the downtime and economic loss due to fire can then be evaluated.

REFERENCES

AASHTO. (2017). LRFD—Road tunnel design and construction guide specification. American Association of State Highway and Transportation Officials, Washington, DC.

Abramowicz, M., and Kowalski, R. (2005). "The influence of short time water cooling on the mechanical properties of concrete heated up to high temperature." Journal of civil engineering and management, 11(2), 85-90.

ACI. (2013). Report on nondestructive test methods for evaluation of concrete in structures. American Concrete Institute Committee 228, Farmington Hills, MI.

ACI. (2016). ACI 562-16: Code Requirements for Assessment, Repair, and Rehabilitation of Existing Concrete Structures and Commentary. American Concrete Institute Committee 228, Farmington Hills, MI.

ACI. (2019). Building code requirements for structural concrete (ACI 318-19). Farmington Hills, MI, USA: American Concrete Institute; 2019.

Ahmad, S., Sallam, Y. S., and Al-Hawas, M. A. (2014). "Effects of key factors on compressive and tensile strengths of concrete exposed to elevated temperatures." Arabian journal for science and engineering, 39(6), 4507-4513.

Akaike, H. (1974). "A new look at the statistical model identification." IEEE transactions on automatic control, 19(6), 716-723.

Al-Jabri, K. S., Waris, M. B., and Al-Saidy, A. H. (2016). "Effect of aggregate and water to cement ratio on concrete properties at elevated temperature." Fire and Materials, 40(7), 913-925.

Albrektsson, J., Flansbjer, M., Lindqvist, J.E., Jansson, R. (2011). Assessment of concrete structures after fire. SP Technical Research Institute of Sweden.

Anagnostopoulos, N., Sideris, K., and Georgiadis, A. (2009). "Mechanical characteristics of self-compacting concretes with different filler materials, exposed to elevated temperatures." Materials and structures, 42(10), 1393-1405.

Anwar Hossain, K. M. (2006). "Macro-and microstructural investigations on strength and durability of pumice concrete at high temperature." Journal of materials in civil engineering, 18(4), 527-536.

Arioz, O. (2007). "Effects of elevated temperatures on properties of concrete." Fire safety journal, 42(8), 516-522.

Arioz, O. (2009). "Retained properties of concrete exposed to high temperatures: Size effect." Fire and Materials: An International Journal, 33(5), 211-222.

ASTM. (2020). ASTM C856M - 20 Standard test method for petrographic examination of hardened concrete. ASTM International, West Conshohocken, PA, United States.

Barragán, B., Giaccio, G., and Zerbino, R. (2001). "Fracture and failure of thermally damaged concrete under tensile loading." Materials and structures, 34(5), 312-319.

Bideci, Ö. S. (2016). "The effect of high temperature on lightweight concretes produced with colemanite coated pumice aggregates." Construction and Building Materials, 113, 631-640.

Bingöl, A. F., and Gül, R. (2009). "Effect of elevated temperatures and cooling regimes on normal strength concrete." Fire and Materials: An International Journal, 33(2), 79-88.

Bisby, L., Mostafaei, H., Pimienta, P. (2014). White paper on fire resistance of concrete structures. US Department of Commerce, National Institute of Standards and Technology, Gaithersburg, MD.

BTS: British Tunnelling Society. (2004). Tunnel lining design guide. ICE Publishing.

Bui, N. K., Satomi, T., and Takahashi, H. (2018). "Effect of mineral admixtures on properties of recycled aggregate concrete at high temperature." Construction and Building Materials, 184, 361-373.

Caner, A., Böncü, A. (2009). "Structural fire safety of circular concrete railroad tunnel linings." Journal of structural engineering. 135:1081-92.

CEB-FIP, B. (2007). "Fire Design of Concrete Structures—Materials, Structures and Modelling." State of art report. Lausanne.

Cekerevac C, Laloui L. Experimental study of thermal effects on the mechanical behaviour of a clay. International Journal for Numerical and Analytical Methods in Geomechanics. 2004;28:209-28.

CEN. (2004). Eurocode 2: Design of concrete structures – Parts 1–2: General rules –Structural fire Design (EN 1992-1-2). Brussels, Belgium: European Committee.

CEN. (2005). Eurocode 3: Design of steel structures - Part 1-2: General rules - Structural fire design (EN 1993-1-2). Brussels, Belgium: European Committee.

Chan, Y., Peng, G., and Anson, M. (1999). "Residual strength and pore structure of high-strength concrete and normal strength concrete after exposure to high temperatures." Cement and concrete composites, 21(1), 23-27.

Chang, Y.-F., Chen, Y.-H., Sheu, M.-S., and Yao, G. C. (2006). "Residual stress–strain relationship for concrete after exposure to high temperatures." Cement and concrete research, 36(10), 1999-2005.

Chen, B., Li, C., and Chen, L. (2009). "Experimental study of mechanical properties of normal-strength concrete exposed to high temperatures at an early age." Fire Safety Journal, 44(7), 997-1002.

Chen, G. M., He, Y. H., Yang, H., Chen, J., and Guo, Y. (2014). "Compressive behavior of steel fiber reinforced recycled aggregate concrete after exposure to elevated temperatures." Construction and Building Materials, 71, 1-15.

Concrete Society. (2008). Assessment, design and repair of fire- damaged concrete structures. Concrete Society, Camber- ley, UK.

CTIF International Assoc. of Fire and Rescue Services. (2016). World fire statistics no 21.

Demirel, B., and Keleştemur, O. (2010). "Effect of elevated temperature on the mechanical properties of concrete produced with finely ground pumice and silica fume." Fire Safety Journal, 45(6-8), 385-391.

Deshpande, A. A., Kumar, D., and Ranade, R. (2019). "Influence of high temperatures on the residual mechanical properties of a hybrid fiber-reinforced strain-hardening cementitious composite." Construction and Building Materials, 208, 283-295.

Deshpande, A. A., Kumar, D., and Ranade, R. (2020). "Temperature effects on the bond behavior between deformed steel reinforcing bars and hybrid fiber-reinforced strain-hardening cementitious composite." Construction and Building Materials, 233, 117337.

Eidan, J., Rasoolan, I., Rezaeian, A., and Poorveis, D. (2019). "Residual mechanical properties of polypropylene fiber-reinforced concrete after heating." Construction and Building Materials, 198, 195-206.

Esen, Y. (2010). "The effect of cure conditions and temperature changes on the compressive strength of normal and fly ash-added concretes." International Journal of Physical Sciences, 5(17), 2598-2604.

Felicetti, R. (2013). "Assessment methods of fire damages in concrete tunnel linings." Fire Technology. 509–29.

FHWA. (2009). Technical manual for design and construction of road tunnels — civil elements. Federal Highway Administration, U.S. Department of Transportation.

fib, I. F. f. S. C. (2008). "Fire design of concrete structures -structural behavior and assessment." International Federation for Structural Concrete, Lausanne, Switzerland.

fib: International Federation for Structural Concrete. (2008). Fire design of concrete structures - structural behavior and assessment. International Federation for Structural Concrete, Lausanne, Switzerland.

Franssen, J-M, Gernay, T. (2017). "Modeling structures in fire with SAFIR®: theoretical background and capabilities." Journal of Structural Fire Engineering. 8:300-23.

Gernay, T., Franssen, J-M. (2012). "A formulation of the Eurocode 2 concrete model at elevated temperature that includes an explicit term for transient creep." Fire Safety Journal. 51:1-9.

Gernay, T., Franssen, J-M. (2016). Safir manual- material properties. Liège, Wallonia, Belgium: Université de Liège – ArGEnCo – Structural Engineering.

Ghaaowd, I., Takai, A., Katsumi, T., McCartney, J.S. (2017). "Pore water pressure prediction for undrained heating of soils." Environmental Geotechnics. 4:70-8.

Ghandehari, M., Behnood, A., and Khanzadi, M. (2010). "Residual mechanical properties of high-strength concretes after exposure to elevated temperatures." Journal of Materials in Civil Engineering, 22(1), 59-64.

Haynes, H. (2017). Fire loss in the United States during 2016, National Fire Protection Association, Quincy, MA.

Hoang, N-D, Nguyen, Q-L, Tran, X-L. (2019). "Automatic detection of concrete spalling using piecewise linear stochastic gradient descent logistic regression and image texture analysis." Complexity:5910625.

Holický, M., and Sýkora, M. "Stochastic models in analysis of structural reliability." Proc., Proceedings of the international symposium on stochastic models in reliability engineering, life sciences and operation management, Beer Sheva, Israel, 8-11.

Hua, N., Elhami Khorasani, N., Tessari, A. (2022a). "Numerical modeling of the behavior of reinforced concrete tunnel slabs during heating and cooling," Engineering Structures, 258: 114135

Hua, N., Elhami Khorasani, N., Tessari, A., Ranade, R. (2022b). "Experimental study of fire damage to reinforced concrete tunnel slabs," Fire Safety Journal, 127: 103504.

Hua, N., Tessari, A., Elhami Khorasani, N. (2021). "Characterizing damage to a concrete liner during a tunnel fire." Tunnelling and Underground Space Technology.109:103761.

Hua, N., Tessari, A., Elhami-Khorasani, N. (2020). "Quantifying uncertainties in the temperature-time evolution of railway tunnel fires." Fire Technology. 361–92.

Hurvich, C. M., and Tsai, C. L. (1993). "A corrected Akaike information criterion for vector autoregressive model selection." Journal of time series analysis, 14(3), 271-279.

Ingham, J. (2009). Forensic engineering of fire-damaged structures. Proceedings of the Institution of Civil Engineers – Civil Engineering,12-7.

ITA. (2000). TA WG2: Guidelines for the Design of shield tunnel lining. International Tunneling Association.

ITASCA Consulting Group Inc. (2017). FLAC3D 6.0: Examples. Minneapolis, USA.

Joulin, C. (2019). Thermo-hydro-mechanical coupling within a geomechanical multiphase model framework with special reference to fractured rock masses in the vicinity of a geological disposal facility for radioactive waste [Doctoral Thesis]. London, UK: Imperial College London.

JSCE Tunnel Engineering Committee. (2007). Standard specifications for tunneling-2006: Shield tunnels. Japan Society of Civil Engineers.

Khan, A.-u.-R., Aziz, T., Fareed, S., and Xiao, J. (2020). "Behaviour and residual strength prediction of recycled aggregates concrete exposed to elevated temperatures." Arabian Journal for Science and Engineering, 45(10), 8241-8253.

Kodur, V.K.R., Agrawal, A. (2016). "An approach for evaluating residual capacity of reinforced concrete beams exposed to fire." Engineering Structures. 110: 293-306.

Kumar, D., and Ranade, R. (2021). "Influence of matrix-modification and fiber-hybridization on high-temperature residual mechanical performance of strain-hardening cementitious composites." Construction and Building Materials, 302, 124157.

Lau, A., and Anson, M. (2006). "Effect of high temperatures on high performance steel fibre reinforced concrete." Cement and concrete research, 36(9), 1698-1707.

Lee, J., Xi, Y., and Willam, K. (2008). "Properties of concrete after high-temperature heating and cooling." ACI Materials Journal, 105(4), 334.

Li, M., Qian, C., and Sun, W. (2004). "Mechanical properties of high-strength concrete after fire." Cement and concrete research, 34(6), 1001-1005.

Luo, X., Sun, W., and Chan, Y. (2000). "Residual compressive strength and microstructure of high performance concrete after exposure to high temperature." Materials and Structures, 33(5), 294-298.

Manepally, C., Fedors, R., Basagaoglu, H., Ofoegbu, G., Pabalan, R. (2011). Coupled processes workshop report. Center for Nuclear Waste Regulatory Analyses.

Martins, David J., Correia, João R., de Brito, Jorge. (2016). "The effect of high temperature on the residual mechanical performance of concrete made with recycled ceramic coarse aggregates" Fire and Materials, 40 (2), 289-304.

Mathew, G., and Paul, M. M. (2014). "Influence of fly ash and GGBFS in laterized concrete exposed to elevated temperatures." Journal of materials in Civil Engineering, 26(3), 411-419.

Mayring, P. (2004). "Qualitative content analysis." A companion to qualitative research, 1(2), 159-176.

McCartney, J., Jafari, N., Hueckel, T., Sánchez, M., Vahedifard, F. (2019). Emerging Thermal Issues in Geotechnical Engineering. p. 275-317.

Ministry of Transportation and Public Works of the Netherlands. (1999). Evaluation of Memorial Tunnel CFD simulations Netherlands: Ministry of Transportation and Public Works of the Netherlands.

Nassif, A. (2006). "Postfire full stress–strain response of fire-damaged concrete." Fire and Materials: An International Journal, 30(5), 323-332.

NCMA: National Codes and Standards Council of the Concrete and Masonry Industries. (1994). Assessing the condition and repair alternatives of fire-exposed concrete and masonry members. Fire protection planning report.

Ngan, Vu. M., Broere, W., Bosch, J.W. (2017). "Structural analysis for shallow tunnels in soft soils." International Journal of Geomechanics. 17: 04017038.

Pacheco, J. N., De Brito, J., Chastre, C., and Evangelista, L. (2019). "Probabilistic conversion of the compressive strength of cubes to cylinders of natural and recycled aggregate concrete specimens." Materials, 12(2), 280.

Phan, L. T., Lawson, J. R., and Davis, F. L. (2001). "Effects of elevated temperature exposure on heating characteristics, spalling, and residual properties of high performance concrete." Materials and structures, 34(2), 83-91.

Poon, C.-S., Azhar, S., Anson, M., and Wong, Y.-L. (2001). "Comparison of the strength and durability performance of normal-and high-strength pozzolanic concretes at elevated temperatures." Cement and concrete research, 31(9), 1291-1300.

Poon, C.-S., Azhar, S., Anson, M., and Wong, Y.-L. (2003). "Performance of metakaolin concrete at elevated temperatures." Cement and Concrete Composites, 25(1), 83-89.

Qureshi, R., Ni, S., Elhami Khorasani, N., Van Coile, R., Hopkin, D., and Gernay, T. (2020). "Probabilistic models for temperature-dependent strength of steel and concrete." Journal of Structural Engineering, 146(6), 04020102.

Rafi, M. M., Aziz, T., and Lodi, S. H. (2018). "Effects of elevated temperatures on residual properties of low-strength concrete." Journal of Testing and Evaluation, 47(5), 3448-3469.

Rama Seshu, D., and Pratusha, A. (2013). "Study on compressive strength behaviour of normal concrete and self-compacting concrete subjected to elevated temperatures." Magazine of concrete research, 65(7), 415-421.

Ren, Q., Wu, Y., Zhang, X., and Wang, Y. (2019). "Effects of fly ash on the mechanical and impact properties of recycled aggregate concrete after exposure to high temperature." European Journal of Environmental and Civil Engineering, 1-17.

Sachin, V., and Suresh, N. (2020). "Residual properties of normal-strength concrete subjected to fire and sustained elevated temperatures: A comparative study." Journal of Structural Fire Engineering.

Sakr, K., and El-Hakim, E. (2005). "Effect of high temperature or fire on heavy weight concrete properties." Cement and concrete research, 35(3), 590-596.

Salahuddin, H., Nawaz, A., Maqsoom, A., and Mehmood, T. (2019). "Effects of elevated temperature on performance of recycled coarse aggregate concrete." Construction and Building Materials, 202, 415-425.

Sancak, E., Sari, Y. D., and Simsek, O. (2008). "Effects of elevated temperature on compressive strength and weight loss of the light-weight concrete with silica fume and superplasticizer." Cement and Concrete Composites, 30(8), 715-721.

Sarhat, S. R., and Sherwood, E. G. (2013). "Residual mechanical response of recycled aggregate concrete after exposure to elevated temperatures." Journal of Materials in Civil Engineering, 25(11), 1721-1730.

Savov, K., Lackner, R., Mang, H.A. (2005). "Stability assessment of shallow tunnels subjected to fire load." *Fire safety journal*. 40:745-63

Schwarz, G. (1978). "Estimating the dimension of a model." The annals of statistics, 461-464.

Sollero, M., Junior, A. M., and Costa, C. (2021). "Residual mechanical strength of concrete exposed to high temperatures–international standardization and influence of coarse aggregates." Construction and Building Materials, 287, 122843.

Sullivan, P., and Sharshar, R. (1992). "The performance of concrete at elevated temperatures (as measured by the reduction in compressive strength)." Fire Technology, 28(3), 240-250.

Tang, W., and Lo, T. (2009). "Mechanical and fracture properties of normal-and high-strength concretes with fly ash after exposure to high temperatures." Magazine of Concrete Research, 61(5), 323-330.

Tanyildizi, H., and Çevik, A. (2010). "Modeling mechanical performance of lightweight concrete containing silica fume exposed to high temperature using genetic programming." Construction and Building Materials, 24(12), 2612-2618.

Tolentino, E., Lameiras, F. S., Gomes, A. M., Silva, C. A., and Vasconcelos, W. L. (2002). "Effects of high temperature on the residual performance of Portland cement concretes." Materials research, 5(3), 301-307.

Torić, N., Boko, I., Juradin, S., and Baloević, G. (2016). "Mechanical properties of lightweight concrete after fire exposure." Structural concrete, 17(6), 1071-1081.

Tufail, M., Shahzada, K., Gencturk, B., and Wei, J. (2017). "Effect of elevated temperature on mechanical properties of limestone, quartzite and granite concrete." International Journal of Concrete Structures and Materials, 11(1), 17-28.

Türkmen, İ., Bingöl, A. F., Tortum, A., Demirboğa, R., and Gül, R. (2017). "Properties of pumice aggregate concretes at elevated temperatures and comparison with ANN models." Fire and Materials, 41(2), 142-153.

Varona, F. B., Baeza, F. J., Bru, D., and Ivorra, S. (2018). "Influence of high temperature on the mechanical properties of hybrid fibre reinforced normal and high strength concrete." Construction and Building Materials, 159, 73-82.

Xiao, J., Fan, Y., and Tawana, M. (2013). "Residual compressive and flexural strength of a recycled aggregate concrete following elevated temperatures." Structural Concrete, 14(2), 168-175.

Xie, J., Zhang, Z., Lu, Z., and Sun, M. (2018). "Coupling effects of silica fume and steel-fiber on the compressive behaviour of recycled aggregate concrete after exposure to elevated temperature." Construction and Building Materials, 184, 752-764.

Yang, H., Zhao, H., and Liu, F. (2018). "Residual cube strength of coarse RCA concrete after exposure to elevated temperatures." Fire and Materials, 42(4), 424-435.

Yaqub, M., and Bailey, C. (2016). "Non-destructive evaluation of residual compressive strength of post-heated reinforced concrete columns." Construction and building materials, 120, 482-493.

Yonggui, W., Shuaipeng, L., Hughes, P., and Yuhui, F. (2020). "Mechanical properties and microstructure of basalt fibre and nano-silica reinforced recycled concrete after exposure to elevated temperatures." Construction and Building Materials, 247, 118561.

Zega, C., and Di Maio, A. (2006). "Recycled concrete exposed to high temperatures." Magazine of Concrete Research, 58(10), 675-682.

Zhang, B., Bicanic, N., Pearce, C., and Balabanic, G. (2000). "Residual fracture properties of normal-and high-strength concrete subject to elevated temperatures." Magazine of concrete research, 52(2), 123-136.

Zhao, H., Liu, F., and Yang, H. (2020). "Residual compressive response of concrete produced with both coarse and fine recycled concrete aggregates after thermal exposure." Construction and Building Materials, 244, 118397.

Zhuang, J., Payyappalli, V. M., Behrendt, A., Lukasiewicz, K. (2017). Total cost of fire in the United States. Fire Protection Research Foundation. Research for the NFPA mission. University at Buffalo, NY.